The University of Sheffield

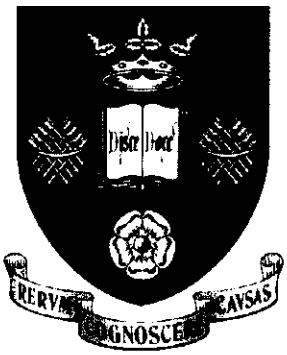

Department of Mechanical Engineering

A theoretical and experimental investigation into the development of coverage in shot peening

Saravanan Karuppanan

Supervisor:
Dr. E. R. de los Rios

A dis e degree of
rity

September 2000

SUMMARY

Shot peening is a mechanical surface treatment process used mainly for the improvement of the fatigue structural integrity of metallic components. In this process, the surface of a part is bombarded with small spherical media called shot, at high velocity, to induce desirable residual compressive stresses and strains within the surface layers of the component.

The effectiveness of the shot peening process is dependent upon the uniformity of the induced compressive residual stresses and the energy transfer that occurs during the impact of the shots with the target surface. In practice, the process efficiency is established by means of coverage, intensity and saturation.

Therefore, the scope of this study is to investigate the development of coverage and its relationship to intensity and saturation of peening. Within the scope, the objectives of the study are to compare and contrast the coverage results obtained experimentally with theoretical models, to establish a relationship between coverage and intensity and to obtain an empirical relationship to predict coverage.

Theoretical models used to predict coverage give mixed results compared to experimental results. The Holdgate model gives a very good coverage prediction whereas the Avrami equation does not.

Coverage development is found to be a function of shot size, impingement angle and target material properties. Intensity and saturation time is found to be dependent upon shot size and impingement angle.

Complete coverage is achieved earlier than the saturation point which is a contrast to the usual assumption that coverage and saturation occurs at the same time. However, a clear relationship could not be established.

An empirical relationship can be used to predict coverage. This relationship, which is a function of the process parameters such as shot size and impingement angle, is established by using multiple regression analysis.

ACKNOWLEDGEMENTS

I would like to express my gratitude to my supervisor, Dr. E.R de los Rios, for his support and interest in the work I have done. I would also like to thank Jose Solis Romero for his assistance and suggestions.

I am also grateful to the University Technology of PETRONAS for sponsoring my studies here.

CONTENTS

LIST OF FIGURES

LIST OF TABLES

NOMENCLATURE

a_j	total area of indentation caused by the peens from the j-th peen source at time δt
b_0 to b_5	regression coefficients
A	area of shot spread
b	regression analysis constants
B	regression analysis constants
$C(t)$	coverage at any particular time
$C(t+\delta t)$	coverage after an increment of time, δt
d_n	nozzle diameter
D	width of shot spread
e	coefficient of restitution
h_{Almen}	hardness of Almen strip
h_{Al2024}	hardness of Al 2024
h_{Al7150}	hardness of Al 7150
k_c	strain rate sensitivity factor of the target material
l	vertical distance between nozzle and sample
L	length of shot spread after 1sec
m	mass of a shot
$\dot{m}$	mass flow rate of the shot
M	mass of shot thrown per unit area per unit time
n_s	number of peen sources
N_p	peen flow rate

$(N_p)_{0.2}$	peen flow rate at 0.2 sec
p	regression analysis constants
P	air pressure
P_m	constant flow pressure of the material
r	average radius of the indentations
$\bar{r}$	average radius of the shots
R	uniform rate of indentation creation
R^2	square correlation of the actual values and the predicted value from the variation
S	total area to be peened
t	time during which the indentations were being created
t_{cov}	time to achieve 98% coverage
t_{sat}	time to achieve saturation in intensity curve
v_p	shot velocity at the instant before impact
V	volume of a shot
x_1	shot diameter (mm) used in regression analysis
x_2	impingement angle (^{0}) used in regression analysis
δN_j	number of peens from the j-th peen source expected to impact the reference area in an interval of time δt
ϕ	divergence angle
ρ	density of the shot
θ	impingement angle

CHAPTER 1

INTRODUCTION

1.1 Background

The failure of engineering structures is an undesirable event for several reasons, which include lost of life, economic losses and the interference with the availability of products and services. Surveys into the causes of in service failures carried out over the last twenty years attribute approximately 80% of catastrophic fractures to fatigue [1].

Effective design strategies require high mechanical efficiency and adequate static and dynamic strengths, for minimum structural weight, in view of the rising costs of materials and energy. Such strategies dictate the optimum use of materials, which is achieved by introducing post-machining treatments to the component.

Thermal and thermochemical treatments have limited applicability, as they appear to discriminate on the material type. Although the mechanical treatments, with exception of shot peening, do not discriminate on the type of materials, their effects are on the component geometry and shape. Shot peening is not only non-discriminatory but also highly versatile and adaptable process.

Shot peening is a mechanical surface treatment process in which the surface of a part is bombarded with small spherical media called shot at high velocity to induce desirable residual compressive stresses and strains within the surface layers of the component.

Shot peening is widely used in the aerospace, automotive, gas turbine and power industries primarily for the improvement of the fatigue structural integrity of metallic components. The residual compressive stress induced by the process will partially nullify the surface tensile stress of external origin and reduce its magnitude.

The net effect is that the likelihood of crack formation and therefore of fatigue failure is reduced.

The effectiveness of the shot peening process is dependent upon the energy transfer that occurs during the impact of shots with the target surface and the uniformity of the induced compressive residual stresses [1]. In practice the process efficiency is evaluated by means of coverage, intensity and saturation. The definition for coverage, intensity and saturation is given in §2.5 and §2.6.

1.2 The Scope of the Dissertation

During shot peening, the intensity of peening and coverage are the two common parameters monitored. Therefore, scope of this study is to investigate the development of coverage and try to establish its relationship to intensity of peening.

Within the above given scope, the aims of the study are to:

(i) Compare and contrast the coverage results obtained experimentally with theoretical models.

(ii) Establish a relationship between coverage and intensity.

(iii) Obtain an empirical relationship to predict coverage from the combination of the peening parameters.

CHAPTER 2

LITERATURE STUDIES

2.1 The History of Shot Peening

Shot peening is a mechanical pre-stressing surface treatment that substantially improves the strength of metals if the process is carefully controlled. The earliest record of mechanical pre-stressing probably predates 2700 BC, as was reported by Bush (1962) [2], when hammered gold helmets were found during the Crusades. Hammering was later used extensively to improve the properties of components such as armours, gun barrels and swords although the reasons for improvement were not understood.

Increased activity in the studies of mechanical pre-stressing and serious search for a scientific analysis of the phenomenon was carried out in the closing of the nineteenth century. In the early of the twentieth century, the World War 1 and World War 2 have encouraged the research to produce high performance and highly reliable steels.

Peening was an well-accepted technology in the early 1920's when handpeening with specific hammers was used in race car industry [3]. However, shot peening as a process of cold working of metal surfaces was only realised in the middle of 1920's as a consequence of the accidental observation on the parts that were sand-blasted for cleaning purposes showed an increased fatigue life.

Development to the process has been significant since then. Some important contributions to this field for the period from about 1920 to 1960 is depicted in Table 2.1 [3].

Author(s) / Institutions	Year	Statements/Proposals
American automotive industries	1926/28	Steel shot blasting
E.G. Herbert	1927	Work hardening due to abrasion ('cloudburst process')
O. Foppl	1929	Cold-hammering improves bending fatigue behaviour of structural steel
German Patent Nr. 573630	1929	Steel shot blasting of springs
E.E. Weibel	1935	Increased fatigue resistance due to shot blasting
J.H Frye G.L. Kehl	1938	Influence of cleaning procedures on fatigue behaviour
R.Z.v. Manteuffel	1939	Improved fatigue strength of sand blasted steel springs
F.P. Zimmerli	1940	Shot blasting and its effect on fatigue fracture life
H. Wiegand	1940	Increased security of surface treated aircraft motor components against fracture
J.O. Almen	1943	Improved fatigue strength of shot peened engine parts; method for measuring peening effects
E.W. Milburn	1945	X-ray diffraction applied to shot peened surfaces
H.O. Fuchs R.L. Mattson	1946	Residual stress measurement at shot peened springs
A.J. Gould U.R. Evans	1948	Improved corrosion fatigue behaviour of shot peened parts
J.C. Straub D. May	1949	Stress peening yields superior enhancements of fatigue strength
R.L. Mattson J.G. Roberts	1959	Analysis of residual stress states induced by strain peening

Table 2.1 : Development of surface strengthening by hammering, shot blasting or shot peening

Since the 1960's, the understanding of the shot peening process has increased significantly, especially in the area of fatigue life improvement. The use of shot peening to improve component fatigue life has also been standardised [4]. However, shot peening process parameters are still selected by means of empirical considerations or by experience. Determining the peening schedules required for optimum shot peening is still a 'black' art.

2.2 Shot Peening Process Mechanism

The mechanism of the shot peening process is a simple concept. It involves [1,5]:

- Small spherical shots made of cast high carbon steel, iron, conditioned cut wire, glass or ceramic are projected with sufficiently high velocity towards the surface of metallic materials. Those shots are propelled either by air pressure or centrifugal force.
- The target component absorbs most of the kinetic energy of the shots as they strike the surface of the component.
- Indentations are formed on the surface of the component because each shot acts as a tiny hammer.
- Local plastic deformation occurs in the material under each indentation during the impact of the shot.
- During rebound of the shot, plastically deformed zone recovers some part of the elastic portion of its total strain.
- The resulting trapped stresses are compressive in nature.
- As the shot peening proceeds until all the surface are indented, these regions of plastic deformation merge to form a permanent global deformed zone in the surface layers of the material.

In most shot peening applications, uniform residual compressive stress in the surface zone is the sole desired effect, as the stresses will resist the formation of fatigue cracks within the component in service. Hence, the fatigue life of the peened

component is improved significantly. A few examples of the type of part, which have shown a good response to shot peening, include crankshafts (900% life increase), gears (1500% life increase), connecting rods (1000% life increase) and etc [6].

Another important application of shot peening is forming of metal parts, changing of component shape into a complex double-curvature, normally by bending towards the stream of shots indenting the component. In shot peen forming, the change in component shape is the desired effect whereas the fatigue life improvement is of secondary importance.

Shot peen forming is generally used when the number of work pieces in a batch is too small to justify investment in mass production processes such as stretching or die bending [7]. The process is widely used to shape the fuselage, wing and empennage surfaces, usually from complex machined panels for a large variety of aircraft [8].

Although the mechanism of shot peening is a simple concept, the process is complex. The results of the shot peening are affected by various process control parameters, target component material properties and peening history of the component. Despite this process complexity, if properly applied, shot peening is one of the best, least expensive (involving the least amount of tooling and start-up costs) and most versatile available method in industry. The advantages of the shot peening process has resulted in the development of various different applications of shot peening as shown in Table 2.2 [9].

SHOT PEENING APPLICATIONS	
METAL FATIGUE	**CORROSION**
Bending	Stress corrosion cracking
Torsion	Intergranular
Axial	Corrosion fatigue
Fretting	Hydrogen cracking
Contact	
Corrosion	**MISCELLANEOUS**
	Work hardening
FORMING	Surface texturing
Aerodynamic	Fretting
Corrective	Galling

Table 2.2 : Shot Peening Applications [9]

2.3 Shot Peening Machine

Industrial shot peening machines may be classified into two major categories depending on the medium that propels the shots. These are air-blast or pneumatic machines and centrifugal peening machines.

The basic components of a typical peening machine are [10]:

(a) shot propelling device which accelerate the shots to the desired velocity

(b) elevator which return the shots to the separator after passing through the projecting device

(c) separator which remove the broken or undersized shots

(d) shot adding device which replace broken and undersized shots with new shots

(e) work conveyor to handle the work so as to subject it to a definite controlled cycle under the shot stream

(f) cabinet to confine the shots within the machine

(g) dust collector to remove the resulting dust from the peening process

2.3.1 Air-blast or pneumatic peening machine

In air-blast peening machines, a high velocity air stream is used to propel the shots through a nozzle onto the component surface. These machines may be subdivided into three categories, depending on the method of introducing the shots into the air stream which are direct-pressure, suction-induction and gravity-induction machines.

In direct-pressure machine [10], shown schematically in Figure 2.1(a), the shots are stored in a pressurised vessel with the pressure maintained as the air which propels the shots. The shots are fed by gravity into a mixing chamber in the pressure vessel, where they are propelled by air pressure and discharged through a nozzle. These machines are usually used for higher intensity shot peening.

In suction-induction machine [10], shown schematically in Figure 2.1(b), compressed air is allowed to expand through a nozzle which is provided with a port or auxiliary tube through which the shots enter the nozzle. The shots are drawn into the air stream by entrainment and then are accelerated by the air, which is travelling at relatively high velocity. These machines are usually used for low intensities, small parts and small quantity shot peening.

In gravity-induction machine [10], shown schematically in Figure 2.1(c), the shots are stored in hoppers located above the cabinet and are introduced to the nozzle by gravity. The nozzles are similar to that of suction-induction type but have adjustable air jets for variable intensity settings. The vertical and horizontal motion of the nozzles allows variable geometry of parts to be shot peened. These machines are suitable for computer monitoring shot peening.

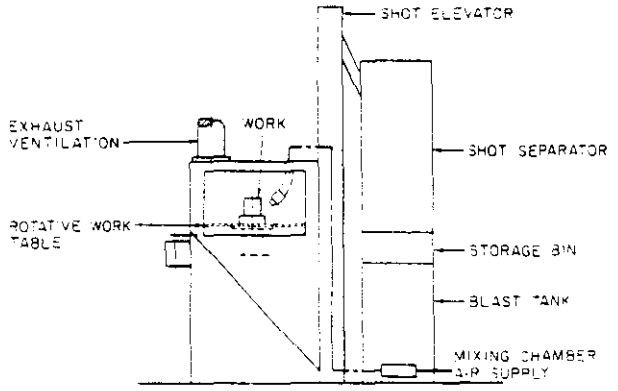

(a)

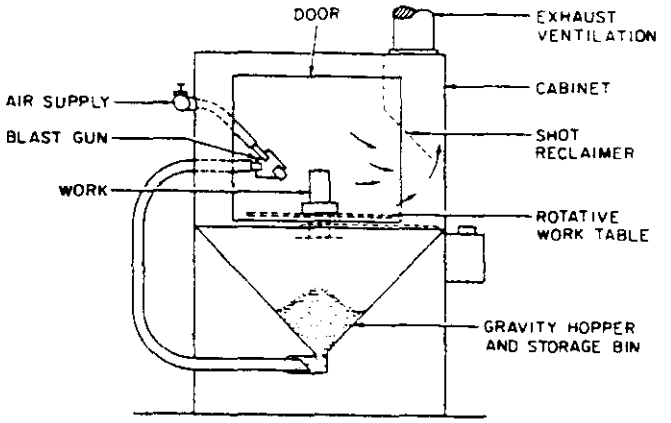

(b)

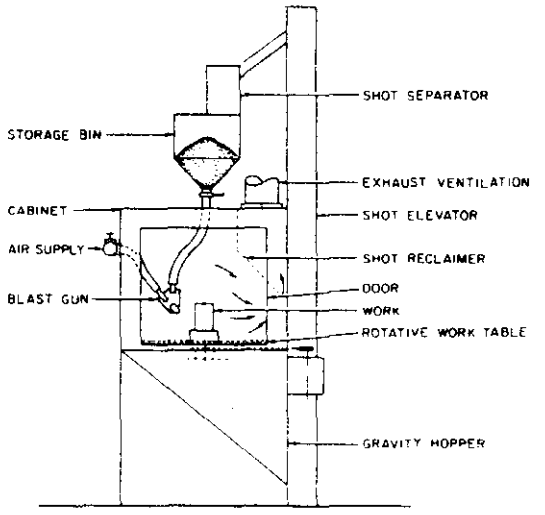

(c)

Figure 2.1 : Schematic diagrams of (a)direct-pressure, (b)suction-induction (c)gravity induction air-blast shot peening machine [10]

2.3.2 Centrifugal peening machine

In centrifugal peening machine [10], shown schematically in Figure 2.2, the shots are propelled by centrifugal force onto the component surface. Gravity or low-pressure air feeds the shots to the hub of a rotating wheel, which has radial vanes or blades. The shots are directed onto the blades of the wheel and then are thrown into a fan-shaped stream by centrifugal force.

For efficient peening, this fan-shaped stream should be as concentrated as possible. An angular adjustment of the control unit is done to get the desired direction of the shot stream. Holdgate [5], reported that the centrifugal machine has two significant advantages over the pneumatic machine. Firstly, it is more efficient in terms of power required for the same peen flow rate and peening intensity. Secondly, it is more suitable for large components because it can deliver more shots in unit time than a pneumatic system.

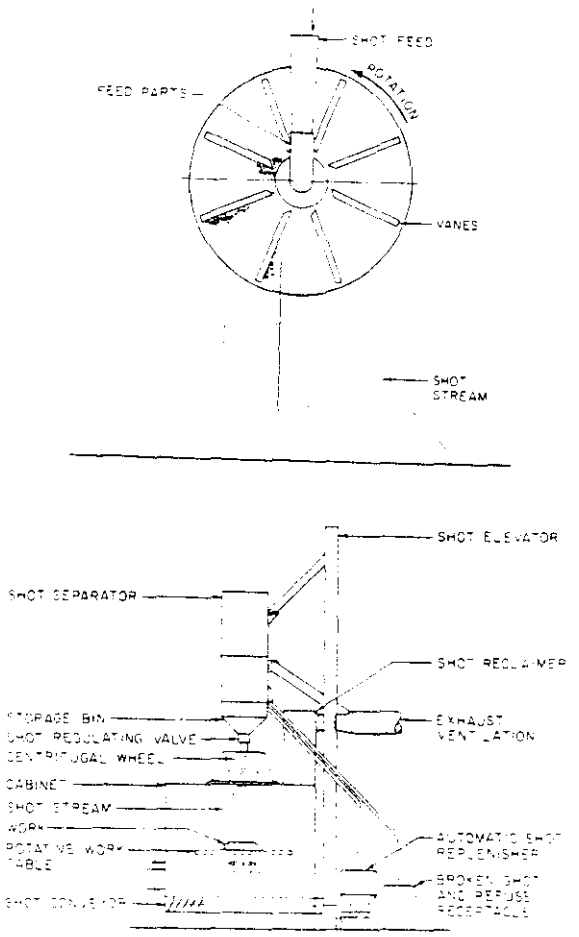

Figure 2.2 : Schematic diagrams of centrifugal wheel (top) used in a centrifugal wheel peening machine [10]

2.4 Shot Peening Media

Several types of media with nominal diameter typically varying between 100μm and 2mm can be used in both types of shot peening machine. These include ferrous and non-ferrous cast shot, cut wire shot, glass beads and ceramic shot. A general classification of peening media is as in Figure 2.3 below [10].

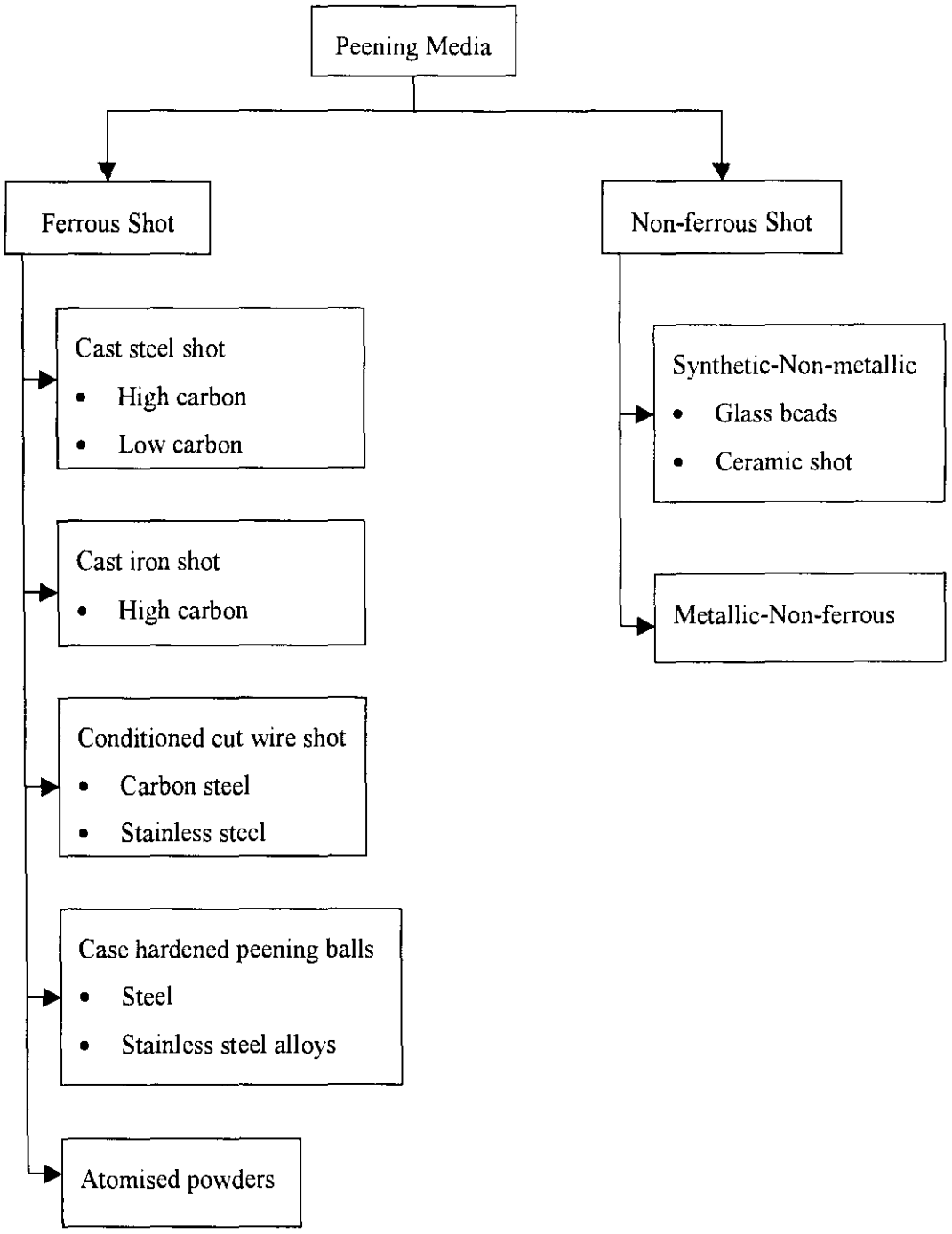

Figure 2.3 : Classification of peening media

The choice of media for shot peening process depends on the type of component part to be peened, the intensity required and the type of shot peening machine [10]. High intensity shot peening require either cast steel or cut wire shot due to their higher mass and durability. Glass and ceramic shot are used for low intensity shot peening. Cast steel shot is the most widely used media especially where high volume of media required such as in centrifugal machines.

All types of media can be used in direct-pressure and gravity-induction machines but suction-induction machines can handle only glass beads, ceramic and fine steel shot (less than 600μm). Conditioned stainless steel cut wire shot, glass beads or ceramic shot can be used when non-ferrous and stainless steel alloy parts are peened to avoid ferrous contamination.

The ideal peening medium should have the following uniform characteristics from particle to particle [11]:

(a) Size : Most consistent size distribution should be used.

(b) Shape (sphericity) : Selected media must resist fracture and formation of sharp edge particles. The acceptable and unacceptable shapes are as shown in Figure 2.4 [4].

(c) Hardness : Peening media should at least as hard as the part to be peened and as hard as Almen Strips.

(d) Density : High-density media are the most durable and fracture resistant.

(e) Durability : Selected media should exhibit the best useful life and resistance to fracture.

(f) Material : Selected media should have the best durability and that leave the lowest amount surface residue.

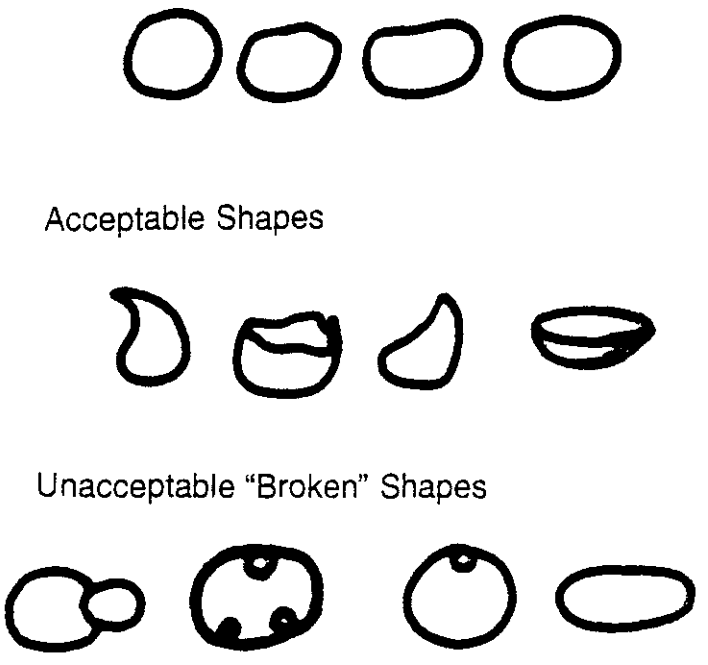

Figure 2.4 : Shot peen media shapes

2.5 Coverage

Coverage is defined as a measure of the area fraction of a component surface that has been impacted in a given peening time, usually expressed as a percentage. In industrial shot peening process, coverage is a measure of the interaction between neighbouring indentations, and hence the uniformity of the residual stresses within the surface layers of the shot peened component.

The complete visual coverage, 100% coverage, is reached when the entire surface of a reference area has been indented. At this point, the residual stresses are assumed to be uniform in the surface layers of the component. Coverage less than 100% are ineffective because of the unpeened surface that contributes to uneven distribution of residual stresses in the surface layers of the component. Coverage above 100% are assumed to be achieved by using multiples of the exposure time necessary to achieve 100% coverage.

Indentations are most likely to occur without overlap in the early stages of shot peening process so that the coverage increases linearly with time. The rate of

coverage decreases with time because the probability of overlap increases. The probability of uncovered area to be covered by a new indentation becomes smaller and smaller with time. Hence the approach to 100% coverage is exponential.

In practice, the 100% coverage can neither be accurately measured nor achieved with certainty after a definite exposure time. Hence, the complete coverage is assumed to occur when the observed coverage reaches 98% [10,12].

Coverage can be assessed qualitatively by visual inspection of the reference area, with a magnifying glass or quantitatively by image analysis or the dyescan tracers technique. Theoretical models have been developed to predict the development of coverage. In this project, the development of coverage will be determined experimentally with the use of an image analysis technique. Two theoretical models, the Avrami equation and the Holdgate model, will also be used to predict the development of coverage.

2.5.1 The Avrami Equation

A theoretical model was reported by Kirk D et.al.[13], which incorporates shot size indentation, peening rate and exposure time for the prediction of coverage. This model was based on the earlier work by Avrami M and therefore was named as the Avrami Equation.

This equation is based on assumptions that each shot particle makes the same size of indentation and that the shot particles arrive at the surface in a statistically random manner but at a rate which is uniform over a significant period of time. Given these assumptions the Avrami equation is as follow:

$$C(t) = 100\left\{1 - \exp\left(-\pi r^2 R t\right)\right\} \quad \ldots\ldots\ldots\ldots\ldots\ldots (1)$$

where

$C(t)$ is the coverage at any particular time

r is the average radius of the indentations

R is the uniform rate of indentation creation

t is the time during which the indentations were being created

The above equation can be modified to accommodate the parameters that are easily determined for a particular peening system. These parameters are as follow:

$$R = \frac{M}{m} \quad \ldots\ldots\ldots\ldots\ldots\ldots (2)$$

where

M is the mass of shot thrown per unit area per unit time

$$M = \frac{\dot{m}}{A} = \frac{\text{mass flow rate of the shots}}{\text{area of shot spread}}$$

m is the mass of a shot

$$m = V\rho$$

$$= \frac{4}{3}\pi\bar{r}^3\rho$$

where

V is the volume of a shot

ρ is the density of the shot

$\bar{r}$ is the average radius of the shots

Therefore the Avrami equation can be re-written as:

$$C(t) = 100\left\{1 - \exp\left(-\pi r^2 \frac{M}{m} t\right)\right\}$$

$$= 100\left\{1 - \exp\left(-\pi r^2 \frac{\dot{m}}{A} \times \frac{1}{4/3\,\pi\bar{r}^3\rho} t\right)\right\}$$

$$= 100\left\{1 - \exp\left(-\frac{3r^2\dot{m}t}{4A\bar{r}^3\rho}\right)\right\} \quad \ldots\ldots\ldots\ldots\ldots\ldots (3)$$

2.5.2 The Holdgate Model (1993)

N.M.D Holdgate [5], in his dissertation, proposed a model, which could be used to predict the coverage in a general peening system. The proposed model is as below:

$$C(t+\delta t) = 1 - [1 - C(t)] \prod_{j=1}^{n_s} \left[1 - \frac{a_j}{S} \right]^{\delta N_j} \quad \ldots\ldots\ldots\ldots\ldots\ldots (4)$$

where

$C(t+\delta t)$ is the coverage after an increment of time, δt

$C(t)$ is the coverage at a known time t

n_s is the number of peen sources

a_j is the total area of indentation caused by the peens from the j-th peen source at time δt

S is the total area to be peened

δN_j is the number of peens from the j-th peen source expected to impact the reference area in an interval of time δt

The model above could be simplified for a single peen source as below:

$$C(t+\delta t) = 1 - [1 - C(t)] \prod_{j=1}^{n_s} \left[1 - \frac{a_j}{S} \right]^{\delta N_j}$$

$n_s = 1$ for a single peen source

$$\therefore C(t+\delta t) = 1 - [1 - C(t)] \prod_{j=1}^{1} \left[1 - \frac{a_j}{S} \right]^{\delta N_j}$$

$$= 1 - [1 - C(t)] \left[1 - \frac{a}{S} \right] \quad \ldots\ldots\ldots\ldots\ldots\ldots (5)$$

2.6 Intensity and Saturation

Intensity correlates the amount of energy transferred during the impact of a typical shot with the work piece and it is related to the kinetic energy of the blast stream [1]. The Almen strip test, which was originally proposed by J.O.Almen, is usually used to quantify the intensity level [14].

Rectangular steel strips of controlled chemical composition and thermal history are shot peened while being held flat. Almen test strips are available in three different thicknesses, which are suitable for different intensity ranges. Almen gauge is used to measure the deflection of the strip in thousands of an inch or hundredths of a millimeter upon release from its fixed position. The deviation from flatness is known as 'Almen Arc Height' and is proportional to the intensity of the kinetic energy in the shot stream.

Saturation refers to the number, uniformity and relative position of the impingements caused by the shot striking the work piece during the exposure time. Saturation is a measure of the effectiveness of the shot peening process. Almen strips can be used to measure the saturation point and is defined as the earliest point on the curve of arc height plotted as a function of the peening time, where doubling the exposure time produces no more than a 10% increase in arc height. Figure 2.5 shows a typical saturation curve.

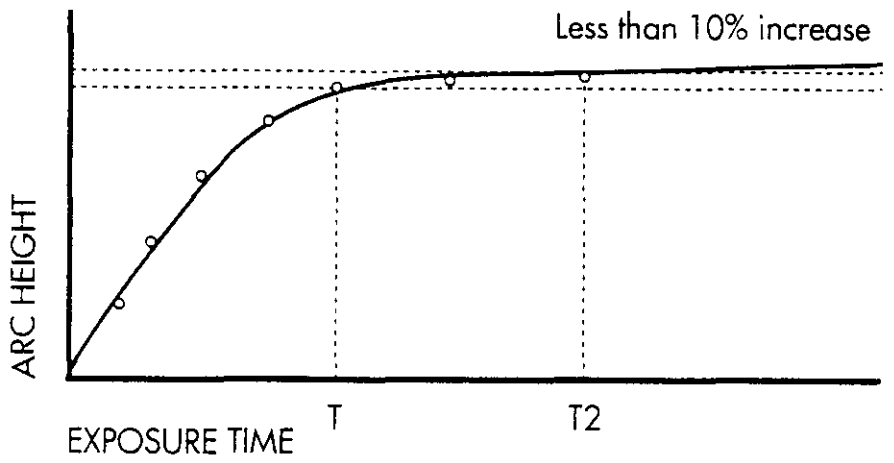

Figure 2.5 : Saturation Curve [4]

CHAPTER 3

METHODOLOGY

3.1 The Experimental Shot Peening Machine

The shot peening machine used in the experiments was the 'Precifeed System' by Tealgate. This machine is the direct-pressure air-blast type machine as described in §2.3.1. Figure 3.1 shows the experimental shot peening machine.

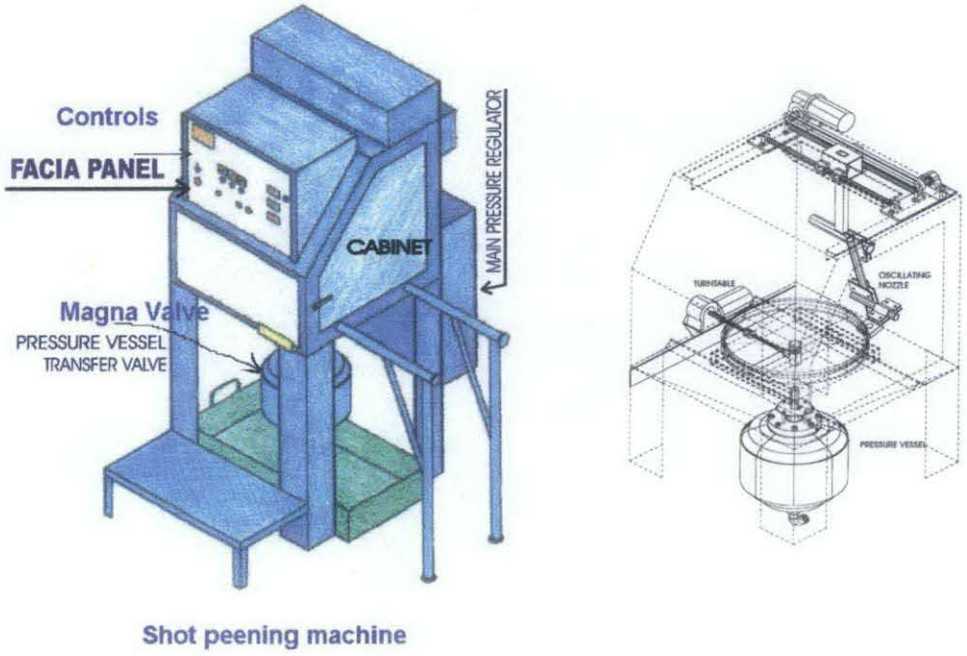

Figure 3.1 : Experimental air-blast shot peening machine [15]

The main components of the machine are:-

(a) Standard blast cabinet

- The capacity is one-meter cube
- Will confine the shots within the machine during experiments

(b) Pressure vessel

- Designed to BS5500

(c) Feed valve system

- Electronically controlled
- The model is 368 MagnaValve

(d) Media valve transfer

- Constructed with a non-metallic cone which is lifted and lowered by the operation of a pneumatic cylinder

(e) Turntable

- Operates either manually or automatically
- Can be selected to remain stationary or rotate at selected speed

(f) Nozzle

- Can be chosen to remain stationary or move at selected speed
- Nozzle frame allows the nozzle direction to be changed over a wide range of angles

(g) Facia control

- All the controls and displays are located on it
- It is facing towards the user

Figure 3.2 shows the schematic diagram of the shot flow within the experimental machine. Compressed air at a desired pressure, which is controlled by a pilot operated pressure regulator, is supplied to the pressure vessel. The pressure of the air is monitored by a pressure transducer and is indicated on a digital display in the facia control.

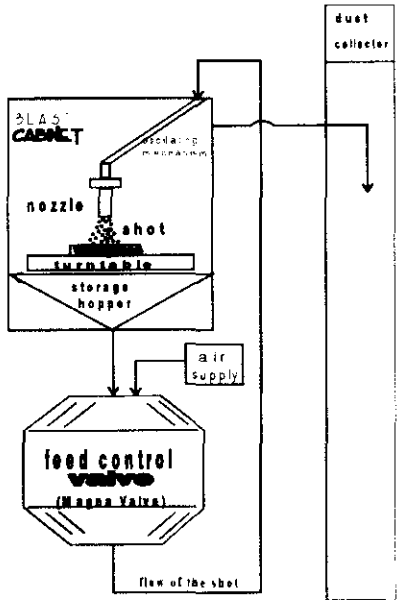

Figure 3.2 : Schematic diagram of media/air flow within the experimental machine [16]

The supplied air is mixed with the shot in the pressure vessel. An electronically controlled feed valve system (MagnaValve), located at the bottom of the pressure vessel, controls the feed rate of the shot in lb/min or kg/min. A signal to the MagnaValve to provide the convenient regulation of the shot flow rate is given by the media transfer valve. The transfer valve is mounted within the control enclosure and is controlled by a multi-turn potentiometer with a vernier dial, which is mounted to the facia control. Flow rate is set by adjusting the vernier dial according to the calibration chart in Table 3.1.

The combined air-media flow then passes through the boost hose into the nozzle mounted at the top of the cabinet. The nozzle directs the shot to the work piece to be peened. The nozzle can be set to remain stationary or move at a selected speed by adjusting the speed vernier dial according to the calibration chart in Table 3.2.

% Vernier	Shot type					
	S110	S170	SCCW 20	SCCW 23	S230	S330
	Shot flow rate : pound/min					
40	5	~	~	~	~	~
45	6	~	~	~	3.7	~
50	8	5.5	~	~	5.6	5
55	~	~	5.3	~	10	~
60	10	7.6	7.8	5.7	11.5	11
70	14	10	10	8.8	~	14.5
75	~	~	~	10.0	~	~
80	20.5	15.4	15.3	13.4	~	17.25
90	26.5	17.2	~	16.8	~	19.5
100	~	~	~	~	39.25	~

Table 3.1 : Calibration chart for flow rate setting

% Vernier	Time to travel 500mm (s)	Speed (mm/s)	Tealgate spec (mm/s)
10	90	6	12
15	40	13	18
20	26	19	24
30	16	31	36
40	11	45	48
60	7	71	72
80	5	100	96
100	4	125	120

Table 3.2 : Calibration chart for nozzle speed setting

The shot drops next to the base of the peening cabinet, where it will be collected in a convergent section for later re-circulation into the shot hopper while the supplied air together with the debris from the peening process are drawn off to a dust collector. The shot will later fall into the pressure vessel.

General specifications of the machine are listed in Table 3.3.

No	Items	Specification
1	PreciFeed pressure vessel capacity	15 litre
2	MagnaValve flow capacity	0 – 50 lb/min
3	MagnaValve full span accuracy	± 5%
4	Turntable rotational speed range	2.9 to 29 rpm
5	Nozzle traverse distance	500 mm
6	Nozzle traverse speed range	12 to 120 mm/sec
7	Nozzle diameter	0.25 in (6.35 mm)
8	Air pressure regulator	Max : 16 bar

Table 3.3 : General specifications of the machine

The operating procedures of the machine for this experiment are briefly described below:

(a) Make sure the desired shot is in the machine.

(b) Clamp the sample to the turntable so that the long axis is left-to-right, that is parallel to the nozzle travelling direction.

(c) Arrange the nozzle so that the blast track will pass centrally over the samples.

(d) Switch the system to manual mode.

(e) Bring the nozzle to the beginning of its travel distance.

(f) Switch the nozzle travel control to OFF.

(g) Check the selected feed rate and switch the MagnaValve to ON.

(h) Check the blast air-media pressure setting.

(i) Check the nozzle speed.

(j) Make sure the nozzle travel control is OFF.

(k) Press the start button and wait until the media-air pressure is constant.

(l) Switch the nozzle travel control to ON.

(m) Stop the machine as the sequencer number increase by 1.

(n) Open the door and bring back the nozzle to its original position.

(o) If inspection is necessary, unclamp the sample and do inspection. To continue, clamp the sample and repeat procedure (h) to (n).

3.2 The Experimental Shot Peening Media

The shot peening media used in the experiments were S110, SCCW20, S230 and S330. 'S' denotes steel, following the British shot grading convention. The specifications of the shot peening media are given in the Table 3.4 below.

Designation	Shot Characteristics	Nominal diameter (mm)	Specification Hardness
S110	Spherical cast steel	0.369	45-52 Rc (410.5-548.5 Hv)
SCCW20	Spherically conditioned steel	0.610	610-670 Hv
S230	Spherical cast steel	0.743	56-58 Rc (615-668 Hv)
S330	Spherical cast steel	1.045	56-58 Rc (615-668 Hv)

Table 3.4 : Specifications of the shot peening media

3.3 The Experimental Target Component

In this study, aluminium 2024-T351 and aluminium 7150-T651 were used for the coverage investigation and A type Almen test strips (cold rolled spring steel SAE 1070) were used for the intensity investigation. The chemical compositions and the monotonic mechanical properties of these materials are listed in Table 3.5(a)-(c) and Table 3.6.

Si	Fe	Cu	Mn	Mg	Cr	Zn
0.5	0.5	3.8-4.9	0.3-0.9	1.2-1.8	0.1	0.25

(a) ALUMINIUM 2024-T351

Si	Fe	Cu	Mn	Mg	Cr	Zn	Zr	Ti
0.12	0.15	1.9-2.5	0.10	2.0-2.7	0.04	5.9-6.9	0.08-0.15	0.06

(b) ALUMINIUM 7150-T651 [17]

C	Mn	P	S	Si	Cr	V	Ni	Mo	Al
0.71	0.63	0.007	0.004	0.17	0.16	0.01	0.01	0.01	0.037

(c) 'A' ALMEN TEST STRIP

Table 3.5 : Chemical composition of the materials (weight percentage)

Material Property	Units	Al 2024-T351	Al 7150-T651	Almen strip
Density	g/cm^3	2.77	2.77	7.86
Poisson's ratio	-	0.33	0.33	0.3
Elastic Modulus	GPa	72.4	71-75	-
Hardness	Hv	170	180	515
Yield stress	MPa	325	400-450	-
Ultimate tensile strength	MPa	470	450-540	-

Table 3.6 : Mechanical properties of the materials

Al 2024 and Al 7150 were used for the coverage investigation because of the following reasons:

(i) Al 2024 and Al 7150 are widely used in aerospace forming applications

(ii) These alloy give clear indentation profiles when shot peened

Dimension of the specimens used for the coverage experiments was 25mm × 19mm × (5~7)mm. The length of 25mm was chosen because for this size the

coverage results are reliable and the nozzle movement across the sample is 0.2s, which makes the analysis easier. The width of 19mm, was chose so that the material could be clamped to the material holder easily. The thickness of 5~7mm was chosen for providing sufficient support behind the point of impact. This will avoid the target material from being elastically deflected and also allows the plastic flow to be constrained within the target component.

The surface of the specimen to be peened for coverage investigation was polished to approximately 1μm of surface roughness. The polished surface would reflect more lights compared to unpolished surface. This characteristic is very important because it gives a better contrast between peened and unpeened regions when observation of coverage was made using a microscope.

Dimension of the Almen strips used was 76.2mm × 19mm × 5mm.

3.4 The Experimental Techniques

3.4.1 Experimental conditions

(a) Coverage

Factors and levels chosen for the investigation of coverage are as in Table 3.7.

Factors	Levels
A. Target Component	1. Al 2024 2. Al 7150
B. Angle of incidence	1. 30^{o} 2. 45^{o} 3. 90^{o}
C. Shot peening media	1. S110 2. SCCW20 3. S230 4. S330

Table 3.7 : Factors and levels for coverage investigation

A total of 24 possible combinations of the four shots, three angles and two target materials were used. These are listed in Table 3.8.

Test No	Shot peening media	Angle of incidence	Target component
1	S110	30°	Al 2024
2	S110	30°	Al 7150
3	S110	45°	Al 2024
4	S110	45°	Al 7150
5	S110	90°	Al 2024
6	S110	90°	Al 7150
7	SCCW20	30°	Al 2024
8	SCCW20	30°	Al 7150
9	SCCW20	45°	Al 2024
10	SCCW20	45°	Al 7150
11	SCCW20	90°	Al 2024
12	SCCW20	90°	Al 7150
13	S230	30°	Al 2024
14	S230	30°	Al 7150
15	S230	45°	Al 2024
16	S230	45°	Al 7150
17	S230	90°	Al 2024
18	S230	90°	Al 7150
19	S330	30°	Al 2024
20	S330	30°	Al 7150
21	S330	45°	Al 2024
22	S330	45°	Al 7150
23	S330	90°	Al 2024
24	S330	90°	Al 7150

Table 3.8 : The test conditions for coverage investigation

The other peening conditions kept constant in all the experiments were:

(i) Shot peen flow rate of 10 lb/min was chosen because it gives a constant mass flow rate for all type of shot peening media under consideration.

(ii) Nozzle velocity of 125mm/sec was chosen since it is the fastest velocity for the machine. This will ensure the suitable coverage increment so that the coverage development could clearly be observed.

(iii) Air pressure of 50 psi.

(iv) Distance between nozzle and sample is 6 in.

(b) Almen intensity

Factors and levels chosen for the investigation of Almen intensity are as in Table 3.9.

Factors	Levels
A. Angle of incidence	1. 30^{o} 2. 45^{o} 3. 90^{o}
B. Shot peening media	1. S110 2. SCCW20 3. S230 4. S330

Table 3.9 : Factors and levels for Almen intensity investigation

A total of 12 test combinations were used as listed in Table 3.10

Test No	Shot peening media	Angle of incidence
1	S110	30^0
2	S110	45^0
3	S110	90^0
4	SCCW20	30^0
5	SCCW20	45^0
6	SCCW20	90^0
7	S230	30^0
8	S230	45^0
9	S230	90^0
10	S330	30^0
11	S330	45^0
12	S330	90^0

Table 3.10 : The test conditions for Almen intensity investigation

Other conditions that were kept constant for all the experiments are as follow:

(i) Shot peen flow rate of 10 lb/min.

(ii) Nozzle velocity of 75mm/sec.

(iii) Air pressure of 50 psi.

(iv) Distance between nozzle and sample is 6 in.

3.4.2 Operating procedure

The operating procedures for coverage and Almen intensity investigation are as follow:

(a) Place the specimen to the holding fixture attached to a stationary turntable.

(b) Clamp the sample to the holding fixture and make sure the turntable is parallel to the nozzle travelling axis.

(c) Arrange the nozzle so that the blast track will pass centrally over the samples.

(d) For the coverage investigation, follow the test conditions as in Table 3.8. Do inspection and measurement of coverage after each pass. Carry out the test until the coverage approach 98%. For Almen intensity investigation, follow the test conditions as in Table 3.10. For each test condition, select the exposure time in a factor of 2 passes (2,4,8,16,....) until the saturation point is achieved.

The operating procedures for determining the spread of the shots are as follow:

(a) Place an aluminium sheet under the nozzle.

(b) Make sure the nozzle travelling control is OFF.

(c) Press the start button and wait until the media-air pressure is constant.

(d) Switch the nozzle travelling control to ON.

(e) Stop the machine as the sequencer number increase by 1.

(f) Take out the aluminium sheet and measure the spread of the shots.

3.4.3 Measurement technique

(a) Coverage

A microscope with magnification ×32 (with a TV camera incorporated) was used to capture images of specimen after each shot peening pass. Three images were captured for each specimen after each shot peening pass. The principle used by the microscope to differentiate between peened and unpeened areas is the amount of light reflected (peened areas are dark while unpeened areas are bright), see Figure 3.3.

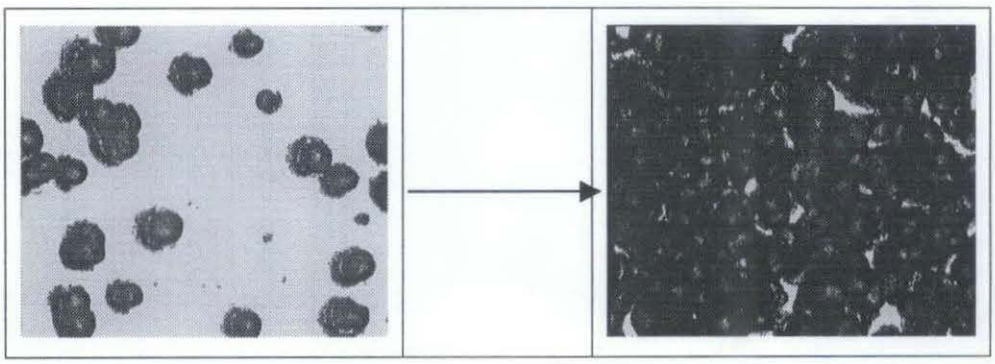

(a) After 1st pass (b) After several passes (98% cov)

Figure 3.3 : Image captured using microscope

The SigmaScan program, an image analysis program, is used to determine the coverage percentage. A threshold value of image contrast for unpeened area is pre-determined before the analysis. Select the unpeened area. Subtract the unpeened area from the total area to find the peened area. The ratio of peened area to the total area is the coverage percentage.

An image from the 1st pass can be used to determine the indentation radius of different shots because the shots are less overlapped at this stage. For an accurate shot indentation result, capture the image using magnification of $\times 100$ and get the average radius from several indentations.

The width of the shot spread can be measured with a ruler.

(b) Almen Intensity and Saturation

Arc heights or intensities were monitored using a standard digital type Almen gauge, with a digital accuracy of 0.0002'' (0.0051mm) [18].

The saturation point is determined by means of regression analysis by using an algorithm developed by Andrew Levers from Airbus UK Ltd. at Chester [16]. The algorithm is transferred to a computer program, which runs employing commercial software called MathCad.

CHAPTER 4

RESULTS

4.1 Coverage

The coverage results determined by an experimental method, the Avrami equation and the Holdgate model are described in §4.1.1~§4.1.3. The coverage development on Al 2024 using shot S230 and at 90^0 angle of impingement is used to demonstrate the application of the above methods in the coverage determination. A summary of all the results is in Appendix 1.

4.1.1 Experimental method

A microscope and a TV camera incorporated with the microscope are used to capture the images of specimens after each shot peening pass. The SigmaScan program is used to determine the coverage percentage. The technique is described in §3.4.3(a). The results are shown in Figure 4.1.

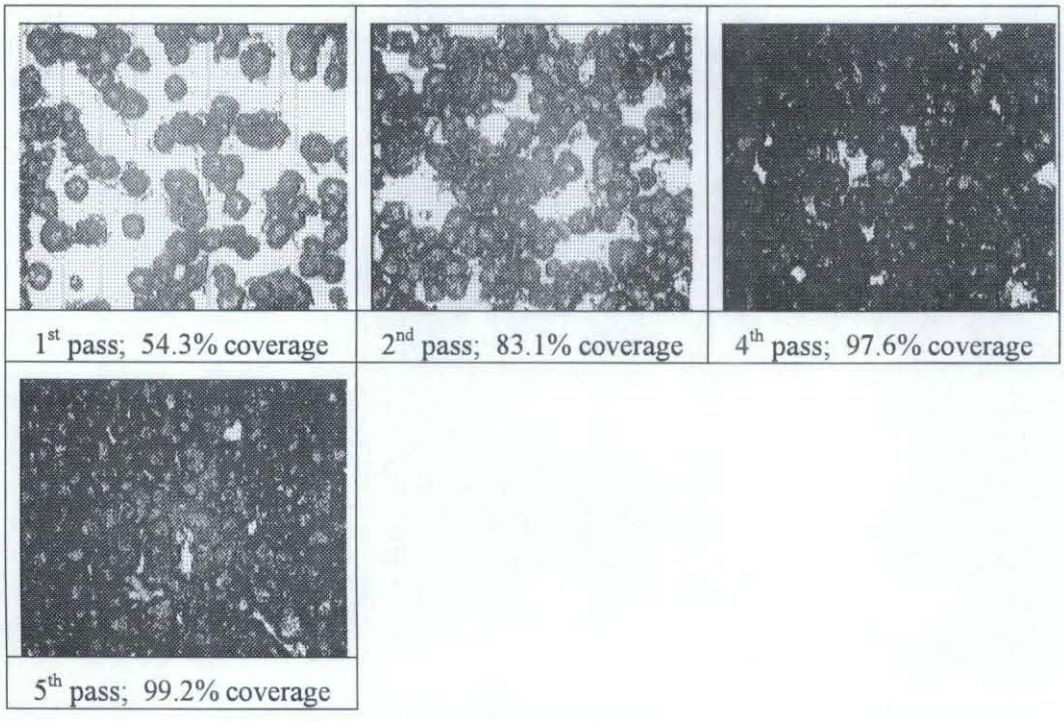

Figure 4.1 : Coverage results determined experimentally

4.1.2 The Avrami Equation (Appendix 2)

The Avrami equation is given below [13]:

$$C(t) = 100\left\{1 - \exp\left(-\frac{3r^2\dot{m}t}{4A\bar{r}^3\rho}\right)\right\} \quad \text{..... (3)}$$

(i) Known parameters

- Mass flow rate of the shot, $\dot{m}$ = 10lb/min = 0.07576 kg/s
- Average radius of the shots, $\bar{r}$ = 0.3715 mm = 0.3715 × 10^{-3} m
- Density of the shot, ρ = 7860 kg/m^3

(ii) Average radius of the indentation, r (Refer to Appendix 2)

(a) Experimental determination

r = 0.299 mm = 0.299 × 10^{-3} m

(b) Theoretical determination [5]

$$r = \left\{\frac{2mv_p^2\bar{r}}{\pi k_c P_m}\left[1 - \frac{3}{8}e^2\right]\right\}^{1/4} \quad \text{..... (6)}$$

where

m = mass of a shot

= volume of a shot × density of a shot

$$= \frac{4}{3}\pi\bar{r}^3\rho = \frac{4}{3}\pi(0.3715\times10^{-3})^3 \times 7860$$

= 1.688 × 10^{-6} kg

v_p = shot velocity at the instant before impact

= 26.5 m/s (Refer to Appendix 2)

k_c = strain rate sensitivity factor of the target material

= 1.36 (Refer to Appendix 2)

P_m = constant flow pressure of the material

= 325 MPa

e = coefficient of restitution

≈ 0 (assuming the rebounding velocity of the shot $\approx$ 0 m/s)

$$\therefore r = \left\{ \frac{2 \times 1.688 \times 10^{-6} \times 26.5^2 \times 0.3715 \times 10^{-3}}{\pi \times 1.36 \times 325 \times 10^{6}} \left[1 - \frac{3}{8} \times 0^2 \right] \right\}^{1/4}$$

$= 0.159 \times 10^{-3}$ m

Note:

The r value determined experimentally will be used in the Avrami equation due to many uncertainties in the parameters of the theoretical equation.

(iii) Area of shot spread, A (Refer to Figure 4.2 & Appendix 2)

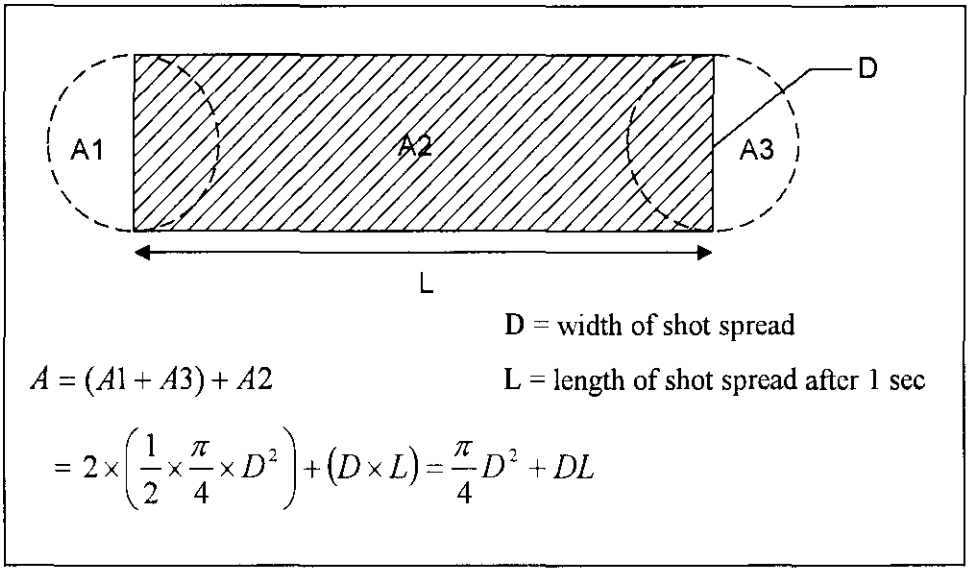

D = width of shot spread

L = length of shot spread after 1 sec

$$A = (A1 + A3) + A2$$

$$= 2 \times \left(\frac{1}{2} \times \frac{\pi}{4} \times D^2 \right) + (D \times L) = \frac{\pi}{4} D^2 + DL$$

Figure 4.2 : Area of shot spread

(a) Experimental determination

D = 21 mm

L = nozzle velocity $\times$ time

= 125 mm/s $\times$ 1 sec = 125mm

$$\therefore A = \frac{\pi}{4} \times 21^2 + (21 \times 125) = 2971\,\text{mm}^2 = 2.971 \times 10^{-3}\,\text{m}^2$$

(b) Theoretical determination

$$D = \frac{d_n + 2l\tan\phi}{\sin\theta} \quad \ldots\ldots\ldots\ldots\ldots\ldots (7)$$

where

d_n = nozzle diameter = 6.4 mm

l = vertical distance between nozzle and sample
= 6 in = 152.4 mm

ϕ = divergence angle = 3^0 (assumption)

θ = impingement angle = 90^0

$$D = \frac{6.4 + (2\times 152.4\times \tan 3^0)}{\sin 90^0} = 22.37\,\text{mm}$$

$$\therefore A = \frac{\pi}{4}\times 22.37^2 + (22.37\times 125) = 3190\,\text{mm}^2 = 3.190\times 10^{-3}\,\text{m}^2$$

Note:

The A value determined experimentally is used in the Avrami equation.

(iv) Application of the Avrami equation

$$C(t) = 100\left\{1 - \exp\left(-\frac{3\times(0.299\times 10^{-3})^2\times 0.07576\times t}{4\times 2.971\times 10^{-3}\times(0.3715\times 10^{-3})^3\times 7860}\right)\right\}$$

$$= 100\{1 - \exp(-4.2427t)\}$$

1st pass coverage = $C(0.2)$ = 57.2%

2nd pass coverage = $C(0.4)$ = 81.7%

3rd pass coverage = $C(0.6)$ = 92.2%

4th pass coverage = $C(0.8)$ = 96.6%

5th pass coverage = $C(1.0)$ = 98.6%

4.1.3 The Holdgate Model [5]

The Holdgate model equation is given below:

$$C(t+\delta t) = 1-[1-C(t)]\left[1-\frac{a}{S}\right] \quad \ldots\ldots\ldots\ldots\ldots\ldots (5)$$

Assume:

1. Time taken for 1 pass of shot peening = δt
2. At $t = 0$, $C(t) = C(0) = 0$

(i) $\frac{a}{S}$ ratio for 1 pass of shot peening

(a) Experimental determination

$\left(\frac{a}{S}\right)_{1\,\text{pass}}$ = coverage ratio after 1st pass of shot peening = 0.543

(b) Theoretical determination (assuming no peen overlapping)

- Time taken to shot peen the sample $= \dfrac{\text{Specimen length (mm)}}{\text{Nozzle speed (mm/sec)}}$

  $= (25/125) = 0.2$ s

- Peen flow rate, $Np \approx \dfrac{3\dot{m}}{4\pi\rho\bar{r}^3} = \dfrac{3\times 0.07576}{4\times\pi\times 7860\times(0.3715\times10^{-3})^3}$

  $= 44880$ peens/sec

- Peen flow rate at 0.2 s, $(N_p)_{0.2} = 44800\times 0.2 = 8976$ peens/0.2 sec

- Peens impacting the specimen $\approx (N_p)_{0.2}\times\dfrac{\text{Specimen width}}{\text{Width of shot spread}}$

  $= 8976\times\dfrac{19}{21} = 8121$ peens

- Indentation created by single peen $= \pi r^2 = \pi\times(0.299)^2$

  $= 0.28086\ \text{mm}^2$

- Total area of indentation created by the peens impacting the specimen, $a = 8121\times 0.28086 = 2280\ \text{mm}^2$

- Total area to be peened, $S = 25\text{ mm} \times 19\text{ mm} = 475\text{ mm}^2$

$$\left(\frac{a}{S}\right)_{1\,\text{pass}} = \frac{2280}{475} = 4.8$$

Note:

The $\left(\frac{a}{S}\right)_{1\,\text{pass}}$ determined experimentally will be used in the Holdgate model.

(ii) Application of the Holdgate model

$$C(t+\delta t) = 1 - \left[1 - C(t)\right]\left[1 - \frac{a}{S}\right]$$

where

$$\delta t = 0.2s; \quad C(t) = 0; \quad \frac{a}{S} = 0.543$$

1^{st} pass coverage ratio = $C(0.2) = 1 - (1-0)(1-0.543) = 0.543$

2^{nd} pass coverage ratio = $C(0.4) = 1 - (1-0.543)(1-0.543) = 0.791$

3^{rd} pass coverage ratio = $C(0.6) = 1 - (1-0.791)(1-0.543) = 0.905$

4^{th} pass coverage ratio = $C(0.8) = 1 - (1-0.905)(1-0.543) = 0.956$

5^{th} pass coverage ratio = $C(1.0) = 1 - (1-0.956)(1-0.543) = 0.980$

4.1.4 Coverage Relationships

(a) Coverage determination by different models

Table 4.1 shows the coverage results determined by different models using shot S230, Al2024 and 30^0 angle of impingement. Figure 4.3 shows the comparison of the coverage results determined by different models.

No of Pass	Coverage (%)		
	Experimental	Holdgate model	Avrami equation
1	41.2	41.2	22.3
2	68.9	65.4	39.6
4	84.0	88.0	63.5
6	95.3	95.9	78.0
8	98.4	98.6	86.7

(Shot : S230; Angle of impingement : 30^0; Material : Al2024)

Table 4.1 : Coverage results determined by different models

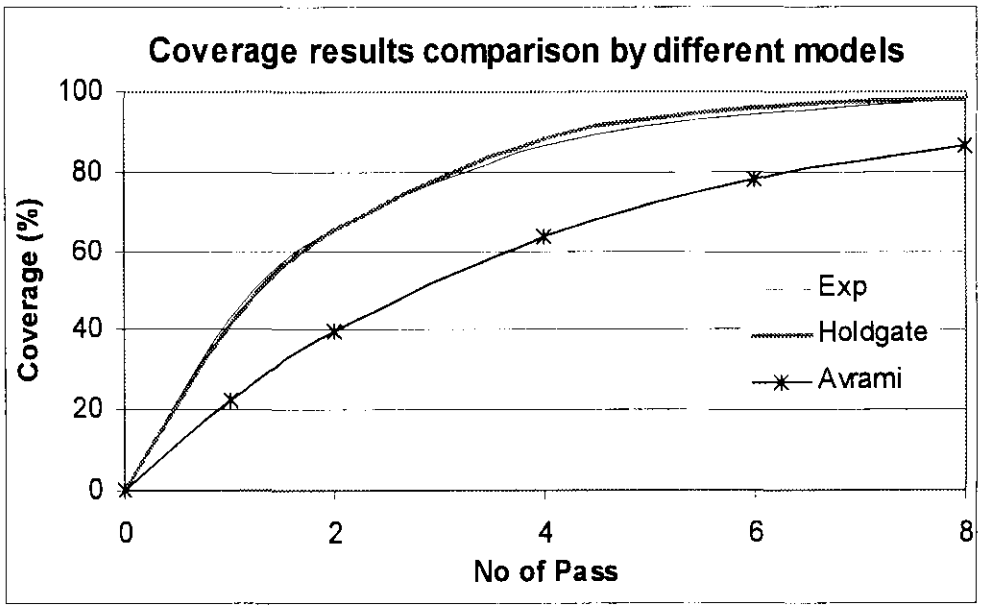

Figure 4.3 : Comparison of coverage results obtained by different models

(b) Coverage development for different shot types

Table 4.2 shows the coverage development for different shots on Al 2024 and 90^0 angle of impingement. Figure 4.4 shows the coverage development for different shot types.

No of Pass	Experimental coverage result (%)			
	S110	SCCW 20	S230	S330
1	96.8	82.3	54.3	42.6
2	99.9	98.9	83.1	62.6
3	~	99.7	91.9	79.7
4	~	~	97.6	86.8
5	~	~	99.2	92.9
6	~	~	~	95.7
7	~	~	~	96.8
8	~	~	~	98.1

Table 4.2 : Coverage results for different shot types on Al 2024 and 90^0 angle of impingement

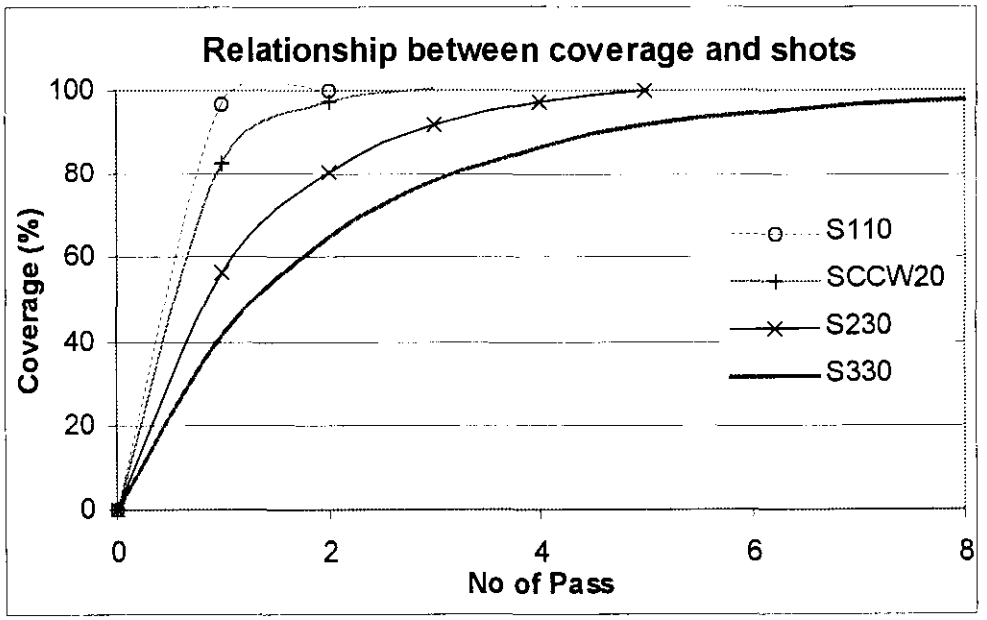

Figure 4.4 : Coverage development using different shot types

(c) Coverage development using different impingement angles

Table 4.3 shows the coverage development on Al2024 using different impingement angles and shot SCCW20. Figure 4.5 shows the relationship between the impingement angle and coverage development.

No of Pass	Experimental coverage result (%)		
	30^0	45^0	90^0
1	66.0	75.4	82.3
2	89.7	94.9	98.9
3	96.6	98.9	99.7
4	99.3	~	~

Table 4.3 : Coverage results for Al2024 using different impingement angles and shot SCCW20

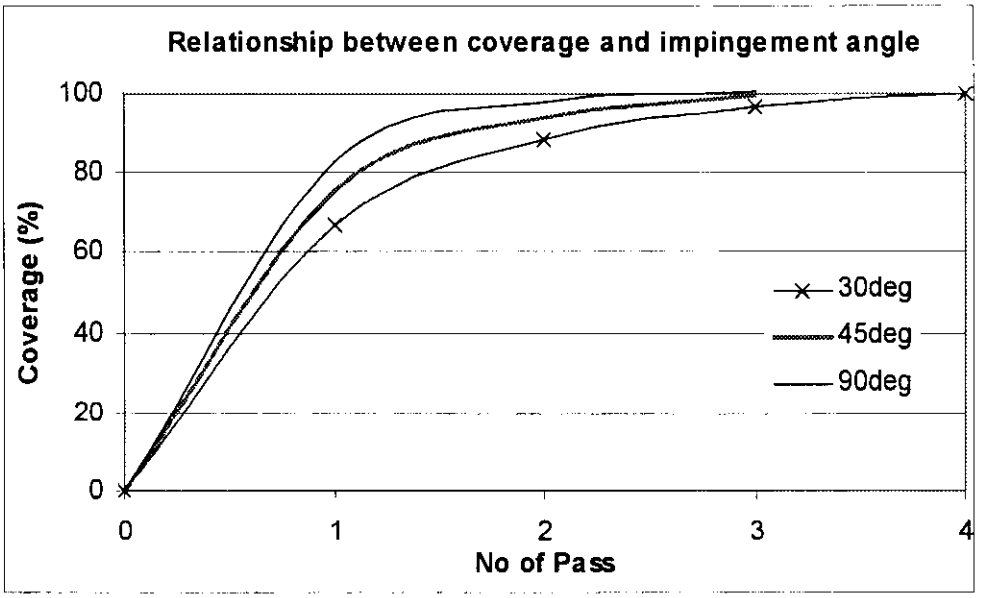

Figure 4.5 : Relationship between coverage development and impingement angle for Al2024

(d) Coverage development on different materials

Table 4.4 shows the coverage development on different materials when using shot S230 and impingement angle of 30^0. Figure 4.6 shows coverage development for different target materials.

No of Pass	Experimental coverage result (%)	
	Al 2024	Al 7150
1	41.2	37.7
2	68.9	55.0
4	84.0	76.6
6	95.3	87.5
8	98.4	95.1

Table 4.4 : Coverage results on different material for shot S230 at 30^0 angle of impingement

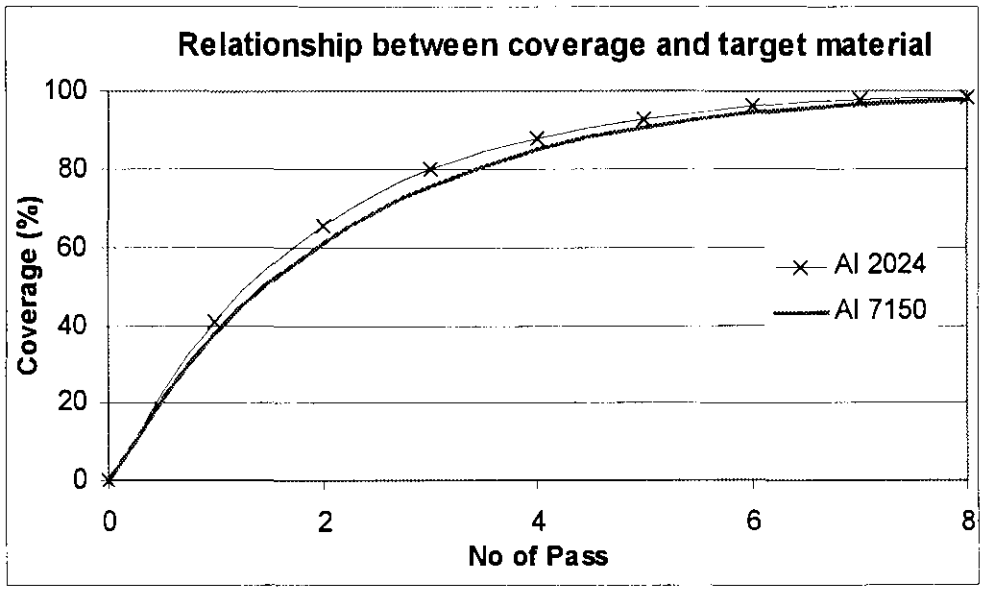

Figure 4.6 : Coverage development on different target materials

4.2 Intensity

Figure 4.7 shows typical intensity/saturation curves. The curves and the saturation points (see §2.6 for definition of saturation point) were determined using an equation proposed by Andrew Levers from Airbus UK Ltd. The equation is [16]:

$$\text{Arc Height} = \frac{B}{(\text{Time} + b)^p} - \frac{B}{b^p} \quad \ldots\ldots\ldots\ldots\ldots\ldots (8)$$

where

B, b & p are regression analysis constants

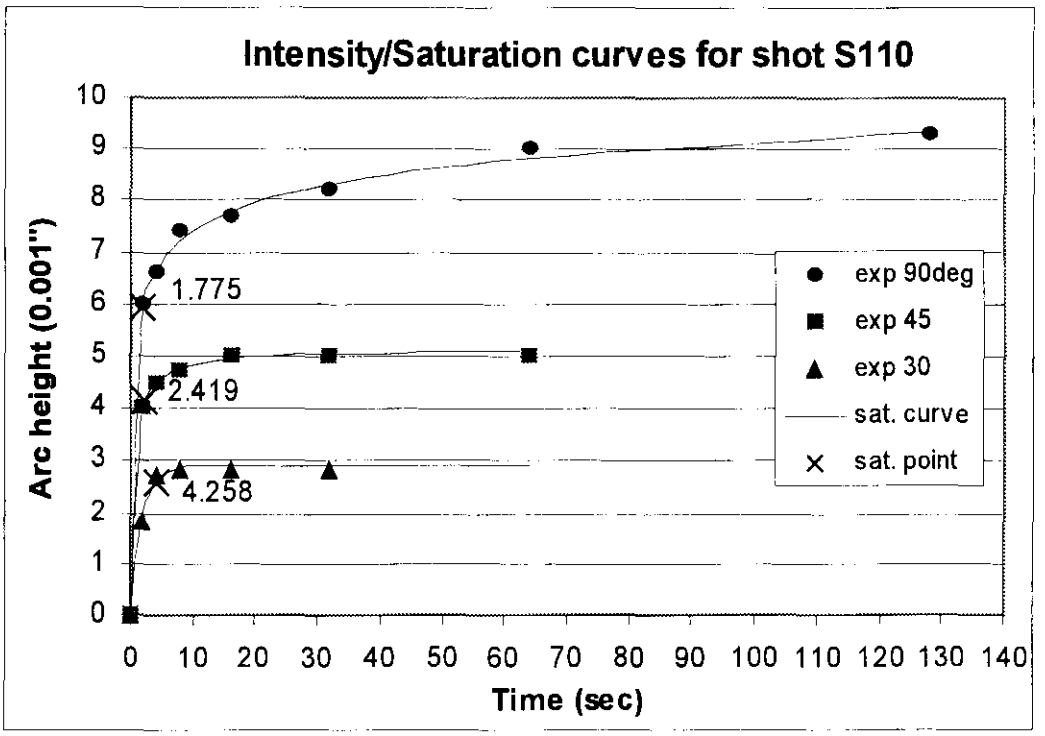

Figure 4.7 : Typical intensity/saturation curves

Table 4.5 shows the intensity and saturation results obtained from the experiments. Appendix 3 shows the graphs of intensity and saturation for all the condition tested.

Shot type	Angle	Arc Height [0.001''] (Intensity)	Saturation time (sec)
S110	30^0	2.61	4.26
	45^0	4.15	2.42
	90^0	5.94	1.78
SCCW20	30^0	4.38	11.32
	45^0	5.77	8.74
	90^0	8.40	6.64
S230	30^0	5.79	19.33
	45^0	7.64	19.89
	90^0	14.74	7.32
S330	30^0	10.71	11.61
	45^0	13.81	8.54
	90^0	25.54	15.70

Table 4.5 : Intensity and saturation results

4.3 Relationship between coverage and intensity

The time to achieve saturation on Almen strips is compared to the time taken to achieve 98% coverage on the test specimens, Table 4.6(a) and Table 4.6(b). The time taken to achieve 98% coverage is determined by using regression equation below:

$$\text{Coverage}(\%) = \frac{B}{(\text{Pass} + b)^p} - \frac{B}{b^p} \quad \ldots\ldots\ldots\ldots\ldots\ldots (9)$$

where

B, b & p are regression analysis constants (Refer to Appendix 4)

Shot	Angle	Sat.time (s) *[x125/75]	Time for 98% cov.(s)	$\frac{t_{cov}}{t_{sat}}$	$\frac{h_{Al2024}}{h_{Almen}}$
S110	30^0	7.10	0.87	0.12	0.33
	45^0	4.03	1.02	0.25	0.33
	90^0	2.96	0.74	0.25	0.33
SCCW20	30^0	18.86	2.01	0.11	0.33
	45^0	14.56	1.60	0.11	0.33
	90^0	11.07	1.28	0.12	0.33
S230	30^0	32.22	4.75	0.15	0.33
	45^0	33.14	3.35	0.10	0.33
	90^0	12.21	2.54	0.21	0.33
S330	30^0	19.35	6.21	0.32	0.33
	45^0	14.24	5.18	0.36	0.33
	90^0	26.17	4.81	0.18	0.33

- Saturation time obtained with nozzle speed of 75mm/s is converted to saturation time with nozzle speed of 125mm/s by multiplying with a factor of 125/75

Table 4.6 (a) : Comparison between saturation and coverage for Al 2024

Shot	Angle	Sat.time (s) *[x125/75]	Time for 98% cov.(s)	$\frac{t_{cov}}{t_{sat}}$	$\frac{h_{Al7150}}{h_{Almen}}$
S110	30^0	7.10	1.81	0.26	0.35
	45^0	4.03	1.10	0.27	0.35
	90^0	2.96	0.86	0.29	0.35
SCCW20	30^0	18.86	2.63	0.14	0.35
	45^0	14.56	1.93	0.13	0.35
	90^0	11.07	1.38	0.12	0.35
S230	30^0	32.22	5.45	0.17	0.35
	45^0	33.14	3.99	0.12	0.35
	90^0	12.21	2.69	0.22	0.35
S330	30^0	19.35	7.92	0.41	0.35
	45^0	14.24	6.83	0.48	0.35
	90^0	26.17	4.48	0.17	0.35

Table 4.6 (b) : Comparison between saturation and coverage for Al 7150

CHAPTER 5

REGRESSION ANALYSIS

5.1 Coverage

A multiple regression analysis [19,20,21] was carried out to predict a/S ratio used in the Holdgate model. A 2nd order polynomial model was utilised (Refer to Appendix 5):

$$\frac{a}{S} = b_0 + b_1 x_1 + b_2 x_2 + b_3 x_1^{\,2} + b_4 x_2^{\,2} + b_5 x_1 x_2 \quad \ldots\ldots\ldots\ldots\ldots\ldots (10)$$

where

x_1 = shot diameter (mm)

x_2 = impingement angle (^{0})

b_0 to b_5 = regression coefficients

Solutions for the regression coefficients b_0 to b_5 were solved on a computer using the Microsoft Excel program. The R^2 value, which represents the strength of the relationship, is the square correlation of the actual values and the predicted value from the variation.

The predictive expressions for a/S ratio for both material and their R^2 values are as follow (Refer to Appendix 5):

Al2024

$$\frac{a}{S} = 1.42615 - 1.72283 x_1 + 1.47869 \times 10^{-3} x_2 + 0.557488 x_1^{\,2} - 4.39349 \times 10^{-6} x_2^{\,2} + 9.70874 \times 10^{-4} x_1 x_2$$

$$R^2 = 0.94$$

Al7150

$$\frac{a}{S} = 1.11595 - 1.47162x_1 + 8.61337\times10^{-3}x_2 + 0.423993x_1^{\,2} - 4.7209\times10^{-5}x_2^{\,2} - 9.70874\times10^{-4}x_1x_2$$

$$R^2 = 0.94$$

5.2 Model validation

Table 5.1 shows the comparison between experimental measurement of a/S ratio and the predicted values generated from the regression model.

No	Shot	Angle	Al 2024			Al 7150		
			Exp	Pre	%error	Exp	Pre	%error
1	S110	30	0.941	0.917	2.5	0.896	0.836	6.7
2		45	0.904	0.940	4.0	0.869	0.907	4.3
3		90	0.968	0.996	2.9	0.939	0.991	5.6
4	SCCW20	30	0.66	0.641	2.9	0.523	0.574	9.8
5		45	0.754	0.667	11.5	0.717	0.641	10.6
6		90	0.823	0.733	10.9	0.829	0.716	13.7
7	S230	30	0.412	0.516	25.2	0.377	0.451	19.6
8		45	0.523	0.544	4.0	0.499	0.516	3.4
9		90	0.543	0.616	13.5	0.535	0.584	9.3
10	S330	30	0.343	0.305	11.0	0.256	0.227	11.5
11		45	0.336	0.338	0.6	0.305	0.287	5.7
12		90	0.426	0.423	0.6	0.322	0.343	6.4

Exp: Experimental value; Pre: Predicted value from regression model

Table 5.1 : Comparison of the a/S ratio determined experimentally and that obtained using the regression model

CHAPTER 6

DISCUSSION

6.1 Coverage

The experimental method used to determine coverage is reliable. High quality images of the specimen are necessary for a reliable and good analysis. Quality images can be captured with a microscope and a TV camera incorporated with the microscope if the surface of the specimen is polished prior to shot peening. The SigmaScan program can be used for a faster and easier coverage determination.

Application of the Avrami equation as in §4.1.2, requires the determination of two parameters which are the indentation radius, r and the shot spread area, A. The theoretical determination of r gives a smaller radius compared to the experimental value. The uncertainties in the theoretical equation parameters, such as shot velocity, strain rate sensitivity factor and flow pressure of the material, may effect the calculated r value. The shot spread area determined theoretically varies slightly from the experimental observation, especially for the 30^0 angle of impingement case. Also from the experimental observation, coarse shot tend to spread more than fine shot.

Application of the Holdgate model as in §4.1.3, requires the determination of the a/S ratio, which is the coverage ratio after an interval time of shot peening. The theoretical prediction of the a/S ratio tends to give a high calculated ratio. This is because the shots are assumed to impact the specimen without overlapping but in reality this does not happen. The coverage ratio after the 1^{st} pass of shot peening determined experimentally, can be used as the a/S ratio required by the Holdgate model for coverage prediction.

Coverage prediction with the Holdgate model agrees much better with the experimental coverage results as compared to Avrami equation, refer to Figure 4.3.

The Holdgate model gives a very good coverage prediction if the a/S ratio is determined accurately. The coverage prediction with the Avrami equation especially for an impingement angle of 45^0 and 30^0 is lower than the experimental value. The application of this equation requires the determination of input parameters such as indentation radius and shot spread area. Inaccurate values of input parameters are the cause of discrepancy in the coverage results.

Table 6.1 shows the advantage(s) and disadvantage(s) of the coverage determination methods, i.e the experimental method, the Holdgate model and the Avrami equation.

Method	Advantage(s)	Disadvantage(s)
Experimental	1. The results are the most reliable. 2. Any problems in peening process can be rectified earlier in the peening schedule.	1. Inspection needed after each interval of shot peening time. It is time consuming and expensive.
Holdgate model	1. Good coverage prediction. 2. Saves time and cost since it needs input that is determined from a single shot peening pass.	1. Inaccurate input parameter will give inaccurate coverage result.
Avrami equation	1. Alternative model of coverage prediction that can be used for comparison purpose.	1. Inaccurate input parameters will give inaccurate coverage result. 2. Prone to error since determination of accurate input parameters is difficult.

Table 6.1 : Advantage(s) and disadvantage(s) of different methods used for coverage determination

Coverage development is faster with shot S110 followed by SCCW20, S230 and S330, refer to Figure 4.4. It means that the coverage rate is faster when using fine shot as compared to coarse shot. At a fixed mass flow rate, the number of shots impacting the sample is higher for fine shot than for coarse shot. Thus, the possibility for fine shot to impact the specimen is higher. This explains the faster coverage rate with fine shot.

Coverage development is faster at impingement angle of 90^0 followed by 45^0 and 30^0, refer to Figure 4.5. The area of shot spread at impingement angle of 90^0 is smaller as compared to 45^0 and 30^0. Thus, the number of shots per unit area is higher at 90^0 impingement angle which increases the possibility for shots to impact the specimen.

Coverage development is faster in Al2024 compared to Al7150, refer to Figure 4.6. Al2024 is softer than Al7150. The indentations created by shots impacting Al2024 are bigger than in Al7150, which explains the faster coverage rate in Al2024.

6.2 Intensity

Intensity values, determined from the arc height of Almen strip, are observed to be higher in peening with coarse shot compared to the fine shot. This was expected since the intensity of peening process is dependent upon the kinetic energy transferred into the specimen. Kinetic energy is a function of velocity and mass of the shot. The velocities measured in this experiment for coarse and fine shot for a particular air pressure and mass flow rate are similar. Thus, coarse shot possesses more kinetic energy than fine shot because it is heavier.

For a particular shot, intensity values obtained for an impingement angle of 90^0 are higher than for 45^0 and this is followed by results obtained for impingement angle of 30^0. The velocity component perpendicular to the surface of target component is higher for impingement angle of 90^0 followed by 45^0 and 30^0. This explains the difference in intensity values.

Saturation is achieved earlier with the fine shot than with coarse shot. The reason for this is that fewer shots are projected onto the Almen strip when using coarse shot as compared to fine shot for a particular mass flow rate.

6.3 Relationship between coverage and intensity

The time taken to achieve 98% coverage in Al2024 and Al7150 is faster than the time taken to achieve saturation in an Almen strip. This was expected because the hardness of the aluminium specimens is lower than the hardness of Almen strips (steel). The ratio of the time taken for 98% coverage to the time taken for saturation, t_{cov}/t_{sat} was observed to be between 0.10~0.36 for Al2024 and 0.12~0.48 for Al7150. A clear relationship between this ratio and the shot type or angle of impingement could not be obtained.

The ratio of aluminium specimen hardness to Almen strip hardness, h_{Al2024}/h_{Almen} and h_{Al7150}/h_{Almen}, was calculated as 0.33 and 0.35 respectively. Basically the t_{cov}/t_{sat} ratio is smaller than h_{Al2024}/h_{Almen} or h_{Al7150}/h_{Almen} ratio with exception of a few cases when using shot S330. This shows that other material factors beside hardness should play a part in coverage development, i.e Young modulus.

6.4 Regression model

Generally, the a/S ratio predicted by the regression model can be used for coverage prediction. The R^2 values, which represent the strength of the relationship, for both Al 2024 and Al 7150, are 0.94. This shows that the relationship is reliable. However, the maximum error for Al 2024 and Al 7150 are 25.2% and 19.6% respectively, which are quite high. Improvement of this relationship could be done if more input data were available for the regression analysis.

CHAPTER 7

CONCLUSION & SUGGESTIONS FOR FUTURE WORK

7.1 Conclusion

Coverage results determined by the Holdgate model agree well with the experimental results. The Avrami equation does not give a good coverage prediction due to the difficulty in determining the accurate input parameters that are used in this equation.

Coverage development is a function of shot size, impingement angle and target material properties. Coverage development is faster using fine shot, at an impingement angle of 90^0 (nozzle perpendicular to the target component) and in soft target component.

Intensity values are dependent upon shot size and impingement angle. The values are high for coarse shot and at an impingement angle of 90^0. At these conditions, the shot possesses high kinetic energy, which will be transferred to the target component during peening process. Saturation time is delayed in coarse shot due to less number of shots impacting the target component.

Complete coverage in Al2024 and Al7150 is achieved earlier than the saturation in Almen strip. The ratio of the time, t_{cov}/t_{sat} is lower than the hardness ratio of specimen to Almen strip, h_{Al2024}/h_{Almen} and h_{Al7150}/h_{Almen} with the exception of some cases with shot S330. Other material factors beside hardness should play a part in coverage development, i.e Young modulus.

An empirical relationship can be used to predict the a/S ratio that is used in the Holdgate model to predict coverage. This relationship, which is a function of shot size and impingement angle, is established by using multiple regression analysis.

7.2 Suggestions for future work

Future development of this work could include:

(i) Investigation of the effect of a/S ratio variation, used in the Holdgate model, on coverage prediction results. The ratio could be varied by varying the mass flow rate, air pressure (shot velocity) or the nozzle velocity.

(ii) Extend the empirical relationship established to predict a/S ratio by including some other process parameters, such as mass flow rate and air pressure.

REFERENCES

1. Dr.S Kyriacou, 'Shot Peening Mechanics, A Theoretical Study', The Sixth International Conference on Shot Peening (ICSP6), pp 505-516, 1996.
2. P.E. Cary, 'History of Shot Peening', The First International Conference on Shot Peening (ICSP1), Pergamon Press, pp 23-28, 1981.
3. K.H Kloss & E.Macherauch, 'Development of Mechanical Surface Strengthening Processes from the Beginning Until Today', Shot Peening : Science-Technology-Application (The Third International Conference on Shot Peening [ICSP3]), Deutsche Gesellschaft fur Metallkunde e.V., pp 3-27, 1987.
4. Military Specification, MIL-S-13165C. Military Specification, 'Shot peening of metal parts', The Wheelabrator Corporation, USA 7 June 1989.
5. N.M.D. Holdgate, 'Peen Mechanics in the Shot Peening Process', PhD thesis, University of Cambridge, October 1993.
6. A.W.E Corporation, 'Shot Peening', 3rd ed. USA: Mishawaka, Indiana, 1947.
7. R.Kopp & H.W Ball, 'Recent Developments in Shot Peen Forming', Shot Peening : Science-Technology-Application (The Third International Conference on Shot Peening [ICSP3]), Deutsche Gesellschaft fur Metallkunde e.V., pp 297-308, 1987.
8. R.J.D Tatton, 'Shot Peen Forming-An Economical Solution', Shot Peening : Science-Technology-Application (The Third International Conference on Shot Peening [ICSP3]), Deutsche Gesellschaft fur Metallkunde e.V., pp 309-318, 1987.
9. Gerald Nachman, 'Modern Shot Peening Technology', Shot Peening : Science-Technology-Application (The Third International Conference on Shot Peening [ICSP3]), Deutsche Gesellschaft fur Metallkunde e.V., pp 37-47, 1987.
10. SAE Fatigue Design and Evaluation Committee, 'SAE Manual on Shot Peening (SAE HS-84)', 3rd ed :Society of Automotive Engineers, Inc., 1991.
11. R.D Gillespie, 'Shot Peening Media : Its Effect on Process Consistency and Resultant Improvement in Fatigue Characteristics', The Fifth International Conference on Shot Peening (ICSP5), pp 81-90, 1993.

12. B.A.(Airbus), 'Process specification (ABP 1-2031)', pp. 1-11, September 93.

13. Kirk D & Abyaneh MY, ' Theoretical Basis of Shot Peening Coverage Control', The Fifth International Conference on Shot Peening (ICSP5), pp 183-190, 1993.

14. Kirk D, 'Interactive Shot Peening Control', The Fifth International Conference on Shot Peening (ICSP5), pp 9-14, 1993.

15. British Aerospace Airbus Division, 'The PreciFeed System by Tealgate's Working Manual', 1998.

16. Jose Solis Romero, 'Optimisation of the Shot Peening Process in terms of Fatigue Resistance', MPhil to PhD transfer report, The University of Sheffield, May 1999.

17. Airbus Industrie Material Specification, 'Aluminium alloy (7150) Specification', 1996.

18. E.I.(EI), '#2 Almen Gage', Owner's Instruction Manual, vol. 1 : EI, pp. 1-16, 1997.

19. Paul G.Hoel, 'Introduction to Mathematical Statistics', John Wiley & sons, Inc., 1971.

20. Irwin Miller & John E.Freund, 'Probability and Statistics for Engineers', Prentice-Hall, Inc., 1977.

21. Morris Hamburg, 'Statistical Analysis for Decision Making', HBC Publishers & Academic Press, 1991.

APPENDIX 1

COVERAGE RESULTS FOR SHOT S110 (Table A)

No	Condition	No of Pass	Coverage (%)		
			Experimental	Holdgate	Avrami
1	Al 2024 S110 30°	1	94.1	94.1	58.8
		2	99.7	99.7	83.1
		3	~	~	93.0
		4	~	~	97.1
		5	~	~	98.8
2	Al 2024 S110 45°	1	90.4	90.4	74.4
		2	99.8	99.1	93.5
		3	~	~	98.4
		4	~	~	99.6
3	Al 2024 S110 90°	1	96.8	96.8	84.5
		2	99.9	99.9	97.6
		3	~	~	99.6
4	Al 7150 S110 30°	1	89.6	89.6	56.5
		2	94.0	98.9	81.1
		3	98.9	99.9	91.8
		4	~	~	96.4
		5	~	~	98.4
		6	~	~	99.3
5	Al 7150 S110 45°	1	86.9	86.9	68.7
		2	99.3	98.3	90.2
		3	~	~	96.9
		4	~	~	99.0
6	Al 7150 S110 90°	1	93.9	93.9	83.7
		2	99.9	99.6	97.4
		3	~	~	99.6

Table A : Coverage results for shot S110

COVERAGE GRAPHS FOR SHOT S110

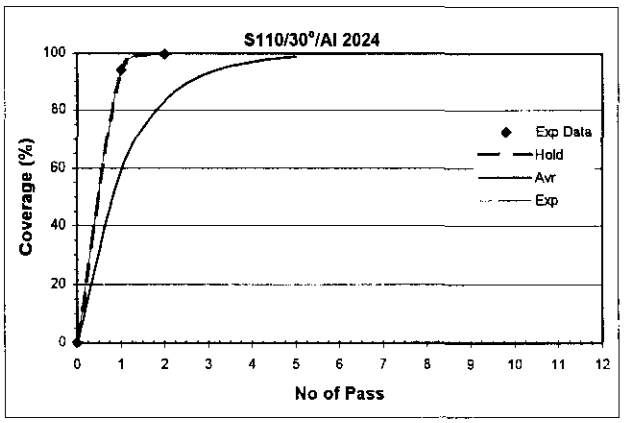

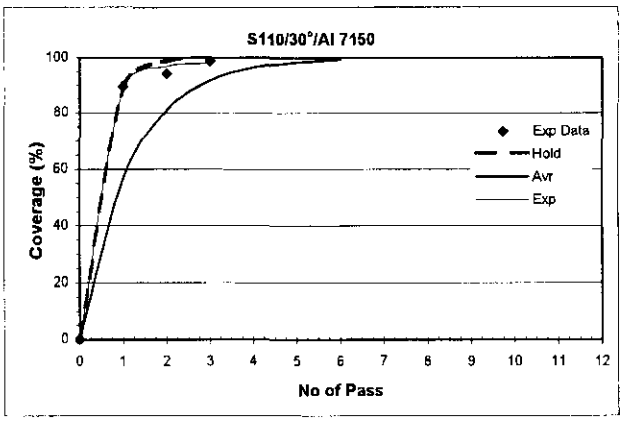

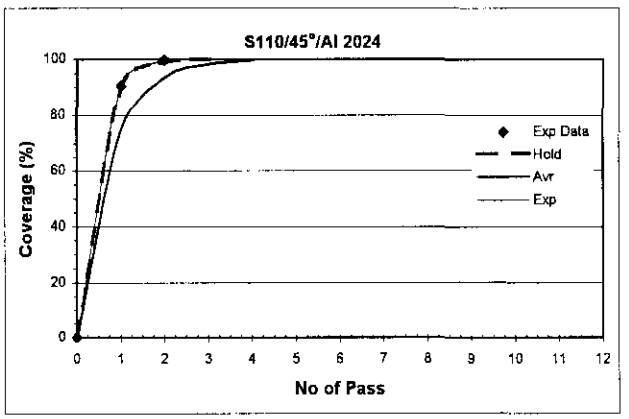

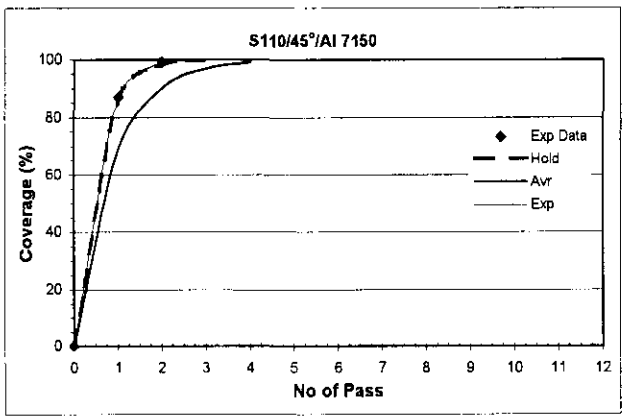

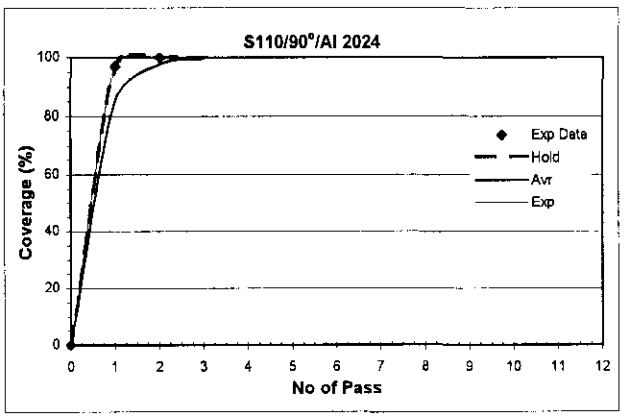

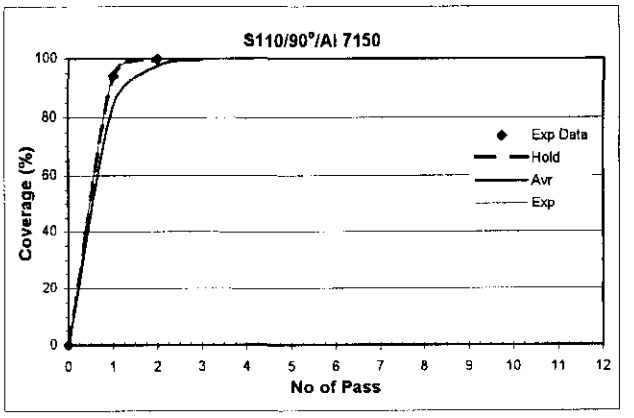

Note: The experimental curves are plotted using equation (9) shown in Section 4.3.

COVERAGE RESULTS FOR SHOT SCCW 20 (Table B)

No	Condition	No of Pass	Coverage (%)		
			Experimental	Holdgate	Avrami
1	Al 2024 SCCW 20 30°	1	66.0	66.0	25.4
		2	89.7	88.4	44.3
		3	96.6	96.1	58.4
		4	99.3	98.7	69.0
		6	~	99.8	82.7
		8	~	~	90.4
		10	~	~	94.6
		12	~	~	97.0
2	Al 2024 SCCW 20 45°	1	75.4	75.4	44.9
		2	94.9	94.0	69.6
		3	98.9	98.5	83.2
		4	~	99.6	90.7
		6	~	~	97.2
		8	~	~	99.1
3	Al 2024 SCCW 20 90°	1	82.3	82.3	56.0
		2	98.9	96.9	80.7
		3	99.7	99.4	91.5
		4	~	~	96.3
		6	~	~	99.3
4	Al 7150 SCCW 20 30°	1	52.3	52.3	24.4
		2	79.3	77.2	42.9
		3	90.5	89.1	56.9
		4	96.3	94.8	67.4
		6	~	98.8	81.4
		8	~	~	89.4
		10	~	~	93.9
		12	~	~	96.5
5	Al 7150 SCCW 20 45°	1	71.7	71.7	45.3
		2	91.2	92.0	70.1
		3	97.5	97.7	83.7
		4	~	99.4	91.1
		6	~	~	97.3
		8	~	~	99.2
6	Al 7150 SCCW 20 90°	1	82.9	82.9	54.1
		2	97.1	97.1	79.0
		3	99.3	99.5	90.4
		4	~	~	95.6
		6	~	~	99.1

Table B : Coverage results for shot SCCW 20

COVERAGE GRAPHS FOR SHOT SCCW 20

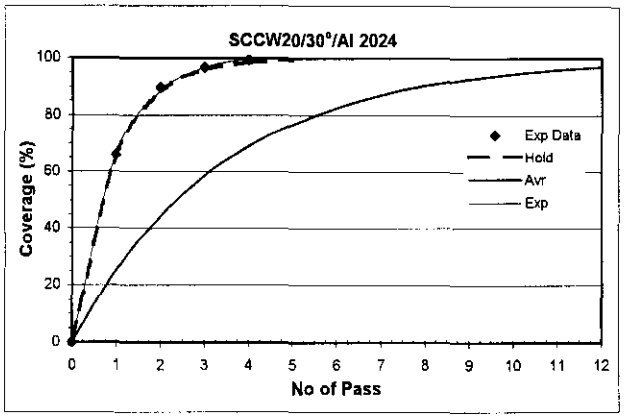

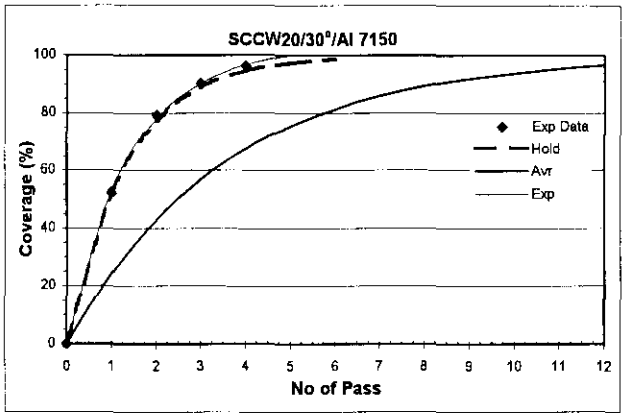

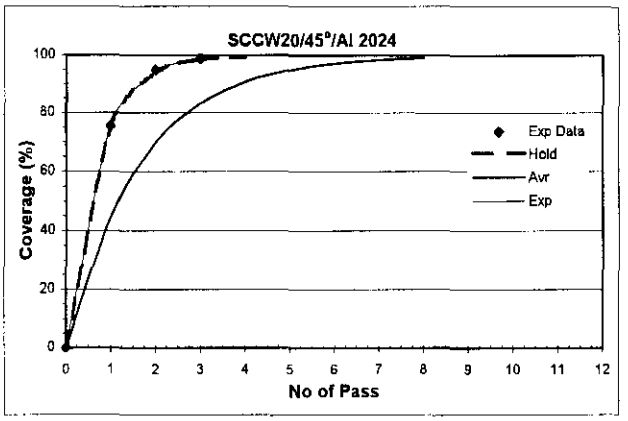

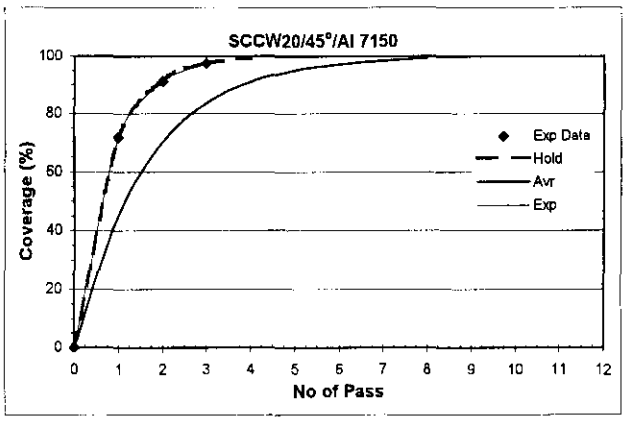

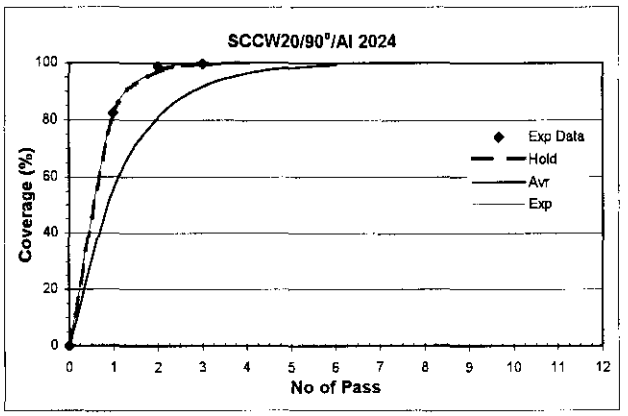

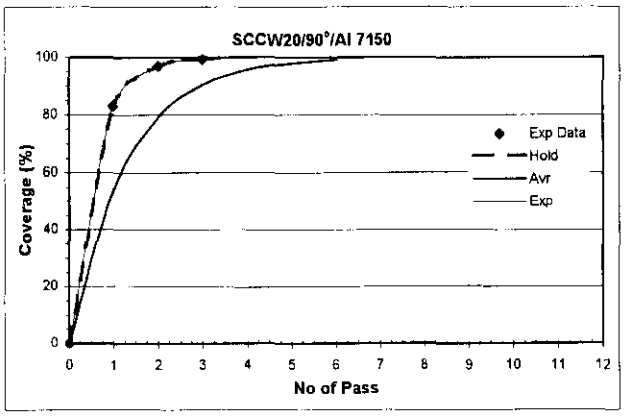

Note: The experimental curves are plotted using equation (9) shown in Section 4.3.

COVERAGE RESULTS FOR SHOT S230 (Table C)

No	Condition	No of Pass	Coverage (%)		
			Experimental	Holdgate	Avrami
1	Al 2024 S230 30°	1	41.2	41.2	22.3
		2	68.9	65.4	39.6
		4	84.0	88.0	63.5
		6	95.3	95.9	78.0
		8	98.4	98.6	86.7
		10	~	99.5	92.0
		12	~	~	95.1
2	Al 2024 S230 45°	1	52.3	52.3	34.4
		2	74.2	77.2	56.9
		4	93.6	94.8	81.5
		6	98.7	98.8	92.0
		8	~	99.7	96.6
		10	~	~	98.5
		12	~	~	99.4
3	Al 2024 S230 90°	1	54.3	54.3	57.2
		2	83.1	79.1	81.7
		4	97.6	95.6	96.6
		5	99.2	98.0	98.6
		6	~	99.1	99.4
		8	~	~	99.9
4	Al 7150 S230 30°	1	37.7	37.7	20.7
		2	55.0	61.2	37.2
		4	76.6	84.9	60.5
		6	87.5	94.2	75.2
		8	95.1	97.7	84.4
		10	~	99.1	90.2
		12	~	~	93.8
5	Al 7150 S230 45°	1	49.9	49.9	31.1
		2	64.7	74.9	52.5
		4	91.0	93.7	77.4
		6	96.3	98.4	89.3
		7	98.2	99.2	92.6
		8	~	99.6	94.9
		10	~	~	97.6
		12	~	~	98.8
6	Al 7150 S230 90°	1	53.5	53.5	53.2
		2	77.7	78.4	78.1
		4	97.0	95.3	95.2
		5	99.4	97.8	97.8
		6	~	99.0	99.0
		8	~	~	99.8

Table C : Coverage results for shot S230

COVERAGE GRAPHS FOR SHOT S230

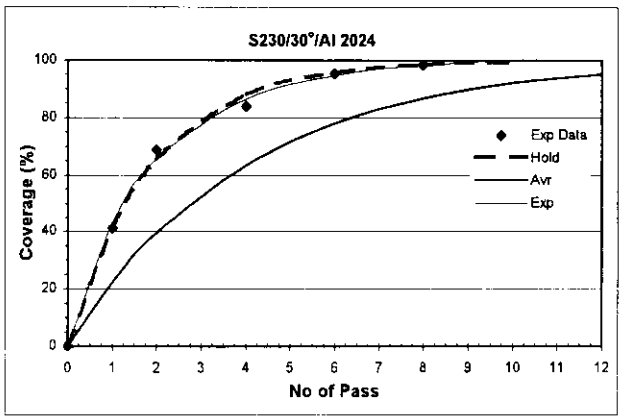

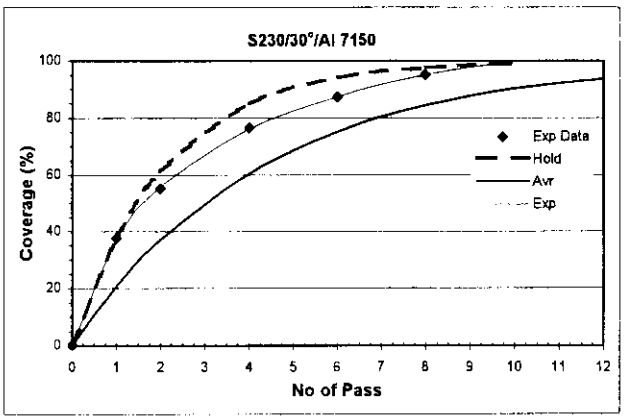

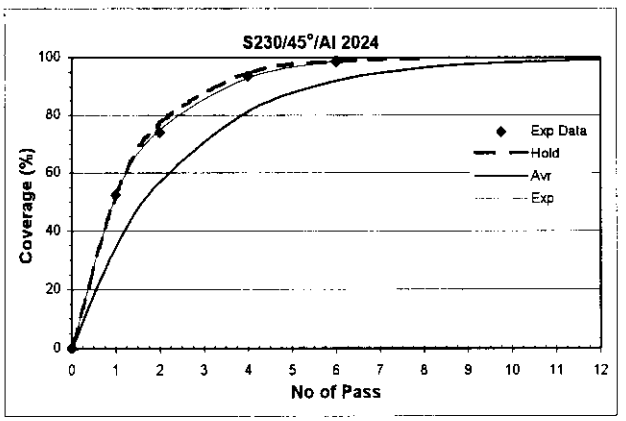

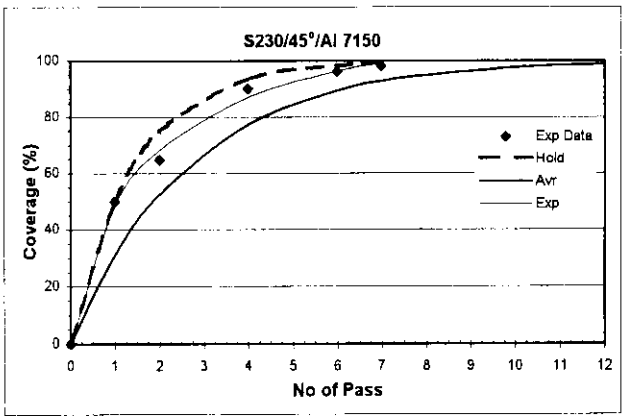

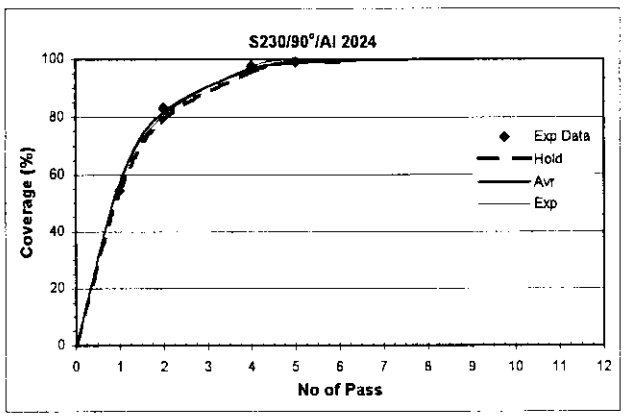

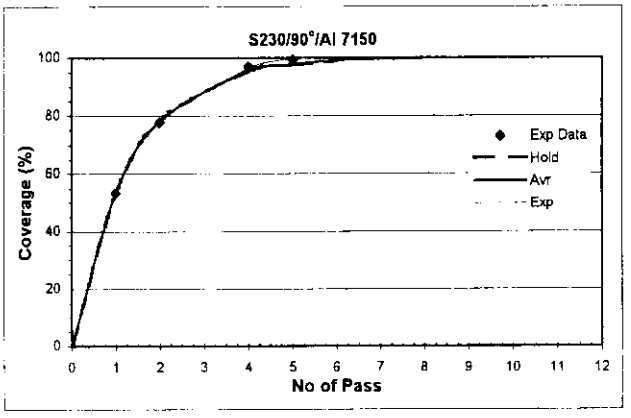

Note: The experimental curves are plotted using equation (9) shown in Section 4.3.

COVERAGE RESULTS FOR SHOT S330 (Table D)

No	Condition	No of Pass	Coverage (%)		
			Experimental	Holdgate	Avrami
1	Al 2024 S330 30°	1	34.3	34.3	15.3
		2	54.7	56.8	28.2
		4	79.7	81.4	48.5
		6	89.1	92.0	63.0
		8	95.2	96.5	73.4
		10	96.7	98.5	80.9
		12	~	99.4	86.3
2	Al 2024 S330 45°	1	33.6	33.6	23.0
		2	57.3	56.0	40.7
		4	79.3	80.6	64.9
		6	92.1	91.4	79.2
		8	96.6	96.2	87.6
		10	97.7	98.3	92.7
		12	~	99.3	95.7
3	Al 2024 S330 90°	1	42.6	42.6	40.0
		2	62.6	67.1	64.0
		3	79.7	81.1	78.4
		5	92.9	93.8	92.2
		6	95.7	96.4	95.3
		8	98.1	98.8	98.3
4	Al 7150 S330 30°	1	25.6	25.6	13.1
		2	44.4	44.6	24.5
		4	70.2	69.4	42.9
		6	80.5	83.0	56.9
		8	86.8	90.6	67.4
		10	90.1	94.8	75.4
		12	~	97.1	81.4
5	Al 7150 S330 45°	1	30.5	30.5	20.2
		2	51.0	51.7	36.3
		4	75.3	76.7	59.4
		6	86.3	88.7	74.2
		8	93.0	94.6	83.5
		10	97.6	97.4	89.5
		12	~	98.7	93.3
6	Al 7150 S330 90°	1	32.2	32.2	37.4
		2	57.0	54.0	60.8
		3	76.9	68.8	75.4
		5	88.7	85.7	90.4
		6	94.8	90.3	94.0
		8	98.4	95.5	97.6
		10	~	97.9	99.1
		12	~	99.1	99.6

Table D : Coverage results for shot S330

COVERAGE GRAPHS FOR SHOT S330

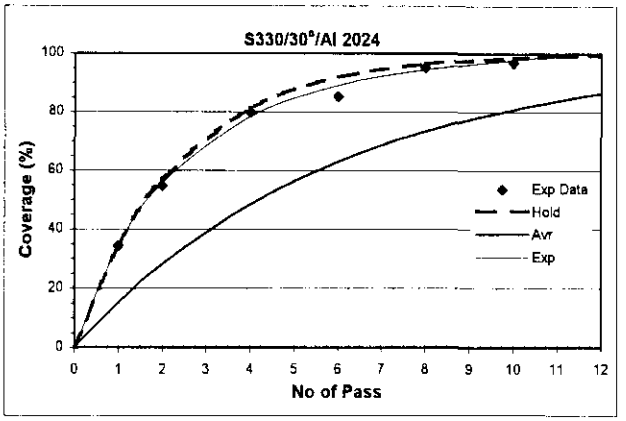

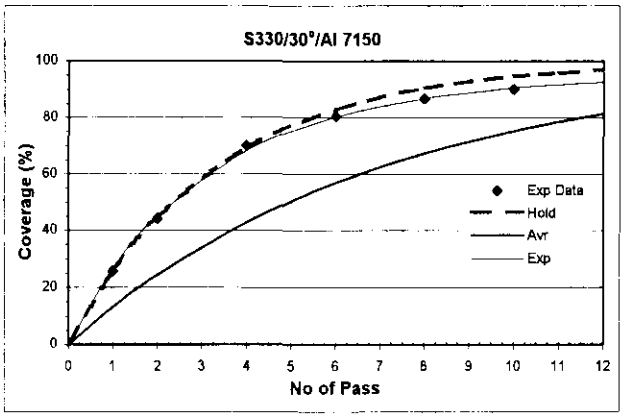

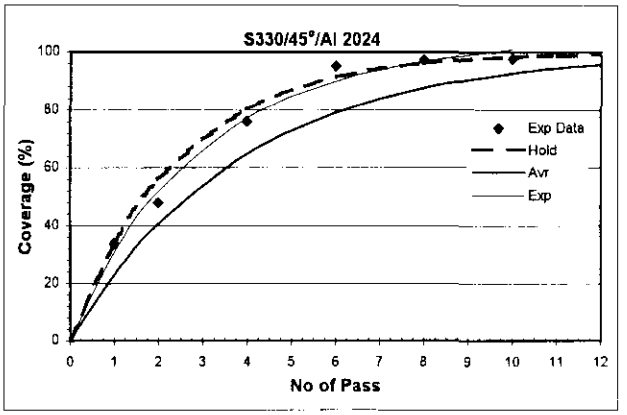

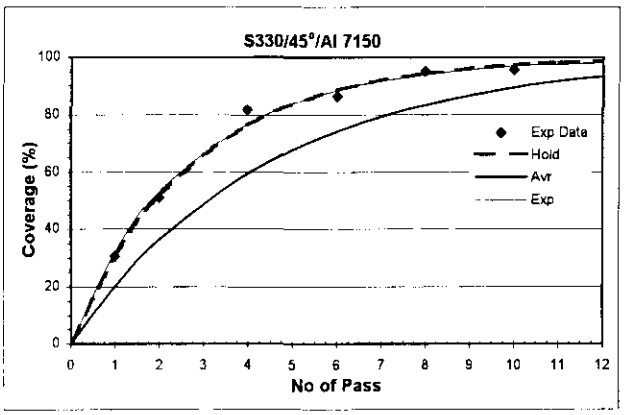

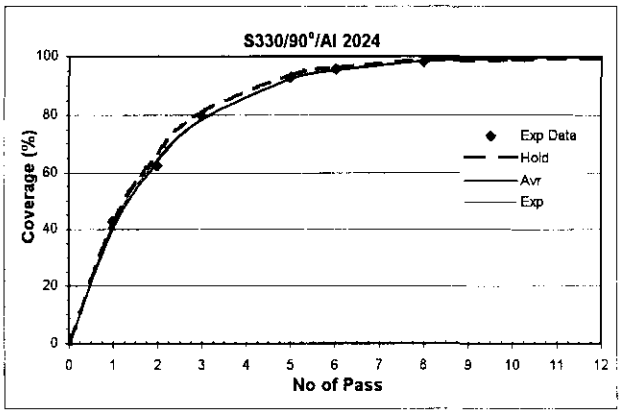

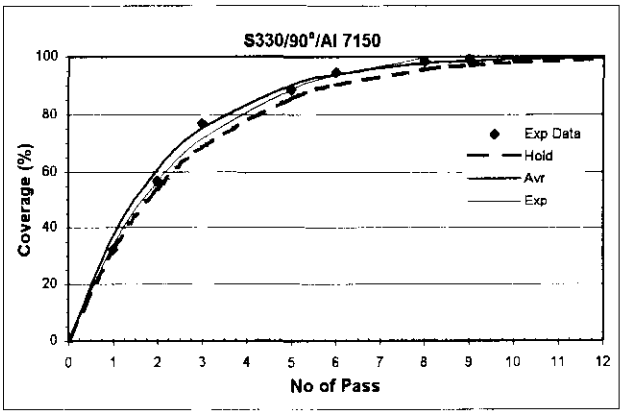

Note: The experimental curves are plotted using equation (9) shown in Section 4.3.

APPENDIX 2

THE AVRAMI EQUATION

$$C(t) = 100\left\{1 - \exp\left(-\frac{3r^2\dot{m}t}{4A\bar{r}^3\rho}\right)\right\} \quad \ldots\ldots\ldots\ldots\ldots\ldots (3)$$

where

r is the average radius of the indentations

$\dot{m}$ is the mass flow rate of the shots

t is the time during which the indentations were being created

A is the area of shot spread

$\bar{r}$ is the average radius of the shots

ρ is the density of the shot

(a) Average radius of the indentations, r

(i) Experimental value (Table E)

Shot	Angle	Al 2024	Al 7150
S110	30^0	0.126 mm	0.122 mm
	45^0	0.143 mm	0.132 mm
	90^0	0.151 mm	0.149 mm
SCCW 20	30^0	0.190 mm	0.186 mm
	45^0	0.206 mm	0.207 mm
	90^0	0.213 mm	0.208 mm
S230	30^0	0.237 mm	0.227 mm
	45^0	0.248 mm	0.233 mm
	90^0	0.299 mm	0.283 mm
S330	30^0	0.344 mm	0.316 mm
	45^0	0.352 mm	0.327 mm
	90^0	0.427 mm	0.409 mm

Table E : Experimental r value

(ii) Theoretical value [5]

$$r = \left\{ \frac{2mv_p{}^2 \bar{r}}{\pi k_c P_m} \left[1 - \frac{3}{8} e^2 \right] \right\}^{1/4} \quad \ldots\ldots\ldots\ldots\ldots\ldots (6)$$

where

m is the mass of a shot

v_p is the shot velocity at the instant before impact

$\bar{r}$ is the average radius of the shots

k_c is the strain rate sensitivity factor of the target material

P_m is the constant flow pressure of the material

e is the coefficient of restitution

- v_p (Refer to Table F)

Shot	Mass flow rate, $\dot{m}$ (g/s)	Velocity, v_p	Velocity at 50psi
S230	6.48	$v_p = 7.072 \times P^{0.58578}$	69.9 m/s
	14.15	$v_p = 7 \times P^{0.57019}$	65.1 m/s
S330	6.48	$v_p = 8.204 \times P^{0.51516}$	61.6 m/s
	14.15	$v_p = 7.589 \times P^{0.52921}$	60.2 m/s
	21.8	$v_p = 7.1809 \times P^{0.53549}$	58.3 m/s

P = air pressure (psi); v_p = shot velocity (m/s)

Table F : Shot velocity at given mass flow rate

For shot S230 & $\dot{m}$ = 10lb/min = 75.76 g/s

Using linear interpolation,

$$v_p = 65.1 + (65.1 - 69.9)\left(\frac{75.76 - 14.15}{14.15 - 6.48} \right) = 26.5 \text{ m/s}$$

For shot S330 & $\dot{m}$ = 10lb/min = 75.76 g/s

Using linear interpolation,

$$v_p = 58.3 + (58.3 - 60.2)\left(\frac{75.76 - 21.8}{21.8 - 14.15}\right) = 44.9 \text{ m/s}$$

NOTE:

1. Linear interpolation is not the best way to estimate the velocity at mass flow rate of 75.76g/s. This is because, the velocity for shot S330 is higher than the shot S230 using this method. Theoretically the velocity for S230 should be slightly higher because it is lighter in mass.

- $\bar{r}$ (Refer to Table G)

Designation	$2\bar{r}$ (mm)	$\bar{r}$ (mm)
S110	0.369	0.1845
SCCW 20	0.610	0.3050
S230	0.743	0.3715
S330	1.045	0.5225

Table G : Shot size

- k_c (Refer to Table H)

Target Material	k_c
Steel	1.28
Brass	1.32
Copper	1.35
Aluminium Alloys	1.36
Nickel	1.38
Lead	1.58
304 Stainless Steel	1.66
301 Stainless Steel	1.89

Table H : Strain rate sensitivity factor [5]

(b) Area of shot spread, A (Figure A & Table I)

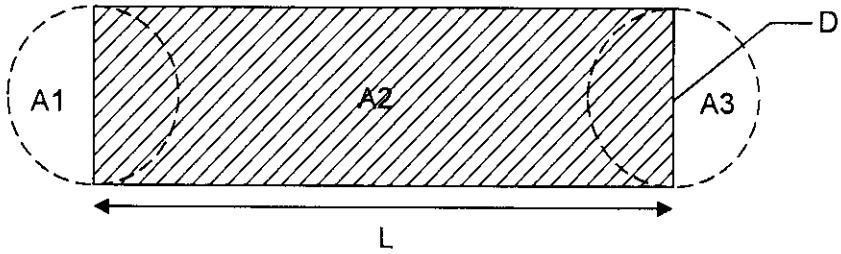

D = width of shot spread

L = length of shot spread after 1 sec

$$A = (A1 + A3) + A2$$

$$= 2 \times \left(\frac{1}{2} \times \frac{\pi}{4} \times D^2 \right) + (D \times L) = \frac{\pi}{4} D^2 + DL$$

Figure A : Schematic representation of shot spread area

Shot	Angle	Exp D (mm)	Theo. D (mm)	Exp A (mm^2)	Theo A (mm^2)
S110	30^0	28	44.8	4116	7176
	45^0	24	31.6	3452	4734
	90^0	20	22.4	2814	3194
SCCW 20	30^0	40	44.8	6257	7176
	45^0	25	31.6	3616	4734
	90^0	20	22.4	2814	3194
S230	30^0	40	44.8	6257	7176
	45^0	28	31.6	4116	4734
	90^0	21	22.4	2971	3194
S330	30^0	45	44.8	7215	7176
	45^0	32	31.6	4804	4734
	90^0	25	22.4	3616	3194

Table I : Results of shot spread area

(c) Summary of the Avrami equations (Table J)

Shot	Angle	Al 2024	Al 7150
S110	30^0	C(t) = 100{1-exp(-4.4397t)}	C(t) = 100{1-exp(-4.1623t)}
	45^0	C(t) = 100{1-exp(-6.8185t)}	C(t) = 100{1-exp(-5.8099t)}
	90^0	C(t) = 100{1-exp(-9.3265t)}	C(t) = 100{1-exp(-9.0811t)}
SCCW20	30^0	C(t) = 100{1-exp(-1.4623t)}	C(t) = 100{1-exp(-1.4012t)}
	45^0	C(t) = 100{1-exp(-2.9756t)}	C(t) = 100{1-exp(-3.0192)}
	90^0	C(t) = 100{1-exp(-4.1078t)}	C(t) = 100{1-exp(-3.8984t)}
S230	30^0	C(t) = 100{1-exp(-1.2604t)}	C(t) = 100{1-exp(-1.1611t)}
	45^0	C(t) = 100{1-exp(-2.1068t)}	C(t) = 100{1-exp(-1.8597t)}
	90^0	C(t) = 100{1-exp(-4.2427t)}	C(t) = 100{1-exp(-3.8008t)}
S330	30^0	C(t) = 100{1-exp(-0.8288t)}	C(t) = 100{1-exp(-0.7014t)}
	45^0	C(t) = 100{1-exp(-1.3071t)}	C(t) = 100{1-exp(-1.1280t)}
	90^0	C(t) = 100{1-exp(-2.5553t)}	C(t) = 100{1-exp(-2.3387t)}

Note : Experimental values of r and A were used as the input parameters.

Table J : Summary of the Avrami equations

APPENDIX 3

INTENSITY/SATURATION CURVES

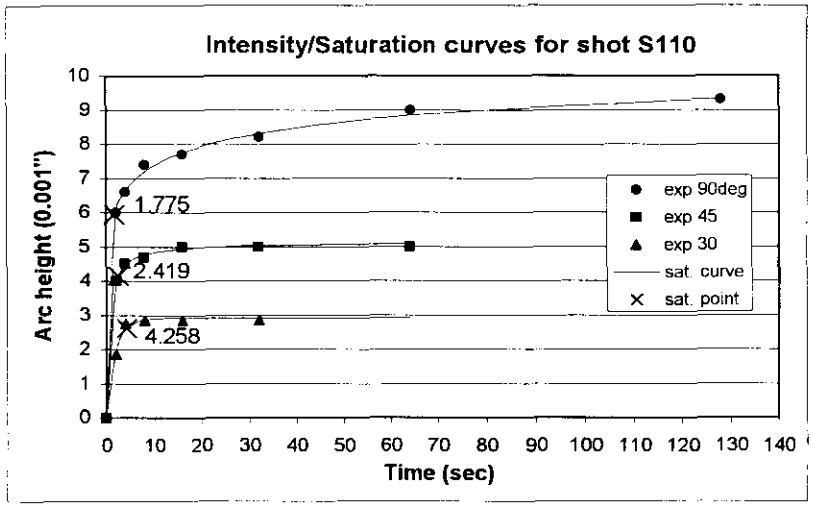

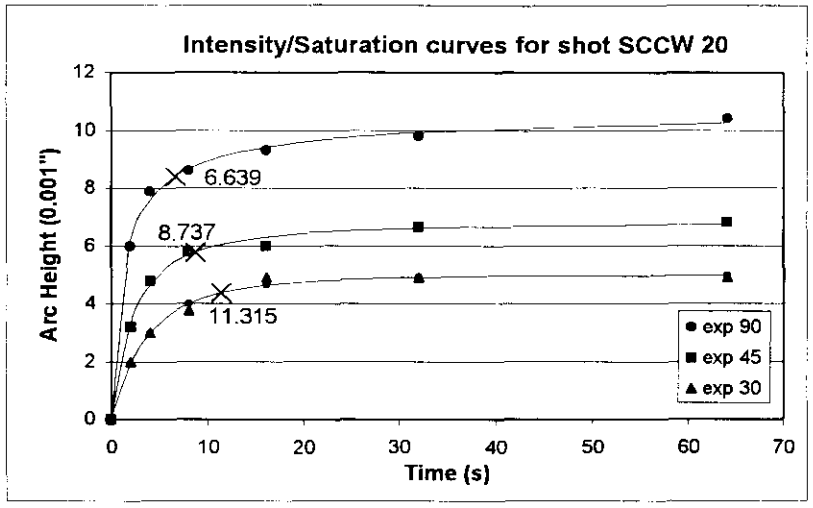

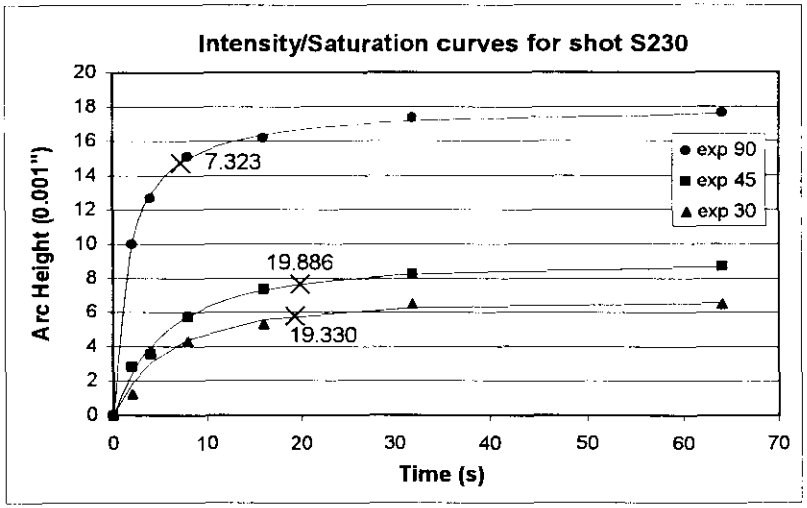

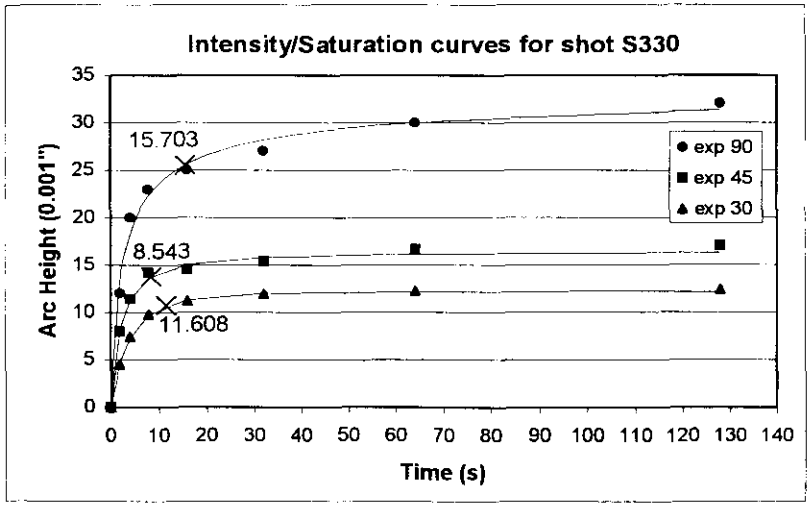

APPENDIX 4

Time taken to achieve 98% coverage is determined by using regression equation below:

$$\text{Coverage}(\%) = \frac{B}{(\text{Pass} + b)^p} - \frac{B}{b^p} \quad \ldots\ldots\ldots\ldots\ldots\ldots (9)$$

where

B, b & p are regression analysis constants (Refer to Table K)

No	Condition	B	b	p	No of Pass for 98% coverage
1	S110/Al2024/30^0	-2.20E+02	1.193	4.414	1.42
2	S110/Al2024/45^0	-3.32E+01	0.516	1.758	1.68
3	S110/Al2024/90^0	-3.15E+01	0.736	3.789	1.21
4	S110/Al7150/30^0	-2.14E+02	1.33E-04	0.039	2.97
5	S110/Al7150/45^0	-5.83E+01	0.712	1.836	1.80
6	S110/Al7150/90^0	-1.03E+05	2.439	7.773	1.41
7	SCCW20/Al2024/30^0	-3.27E+11	8.997	9.961	3.30
8	SCCW20/Al2024/45^0	-2.26E+10	6.884	9.961	2.62
9	SCCW20/Al2024/90^0	-2.43E+09	5.503	9.961	2.10
10	SCCW20/Al7150/30^0	-1.94E+13	13.528	9.961	4.32
11	SCCW20/Al7150/45^0	-3.25E+07	5.567	7.383	3.16
12	SCCW20/Al7150/90^0	-1.48E+09	5.240	9.961	2.26
13	S230/Al2024/30^0	-2.49E+05	6.932	4.023	7.79
14	S230/Al2024/45^0	-1.43E+04	4.391	3.320	5.49
15	S230/Al2024/90^0	-6.96E+12	12.217	9.961	4.17
16	S230/Al7150/30^0	-1.78E+02	1.218	0.430	8.94
17	S230/Al7150/45^0	-1.44E+02	1.150	0.742	6.54
18	S230/Al7150/90^0	-1.45E+12	12.459	9.258	4.42
19	S330/Al2024/30^0	-1.89E+05	8.279	3.550	10.18
20	S330/Al2024/45^0	-3.39E+16	28.591	9.961	8.50
21	S330/Al2024/90^0	-3.76E+14	18.282	9.961	7.89
22	S330/Al7150/30^0	-5.58E+16	30.346	9.961	13.00
23	S330/Al7150/45^0	-1.05E+16	25.555	9.961	11.21
24	S330/Al7150/90^0	-9.78E+15	25.225	9.961	7.36

- Time (in sec) to achieve 98% coverage can be obtained by multiplying the no of pass with a factor of 125/76.2 (converting the aluminium specimens length to the length of Almen Strips)

Table K : Regression analysis constants & Time to achieve 98% coverage

APPENDIX 5

REGRESSION ANALYSIS

2nd order polynomial regression function:

$$y = b_0 + b_1 x_1 + b_2 x_2 + b_3 x_1^2 + b_4 x_2^2 + b_5 x_1 x_2$$

where

$y = \frac{a}{S}$ ratio

b_0 to b_5 = regression analysis coefficients

x_1 = shot diameter (mm)

x_2 = impingement angle

Least square equations for regression coefficients estimation:

$$\sum y = b_o n + b_1 \sum x_1 + b_2 \sum x_2 + b_3 \sum x_1^2 + b_4 \sum x_2^2 + b_5 \sum x_1 x_2$$

$$\sum x_1 y = b_o \sum x_1 + b_1 \sum x_1^2 + b_2 \sum x_1 x_2 + b_3 \sum x_1^3 + b_4 \sum x_1 x_2^2 + b_5 \sum x_1^2 x_2$$

$$\sum x_2 y = b_o \sum x_2 + b_1 \sum x_1 x_2 + b_2 \sum x_2^2 + b_3 \sum x_1^2 x_2 + b_4 \sum x_2^3 + b_5 \sum x_1 x_2^2$$

$$\sum x_1^2 y = b_o \sum x_1^2 + b_1 \sum x_1^3 + b_2 \sum x_1^2 x_2 + b_3 \sum x_1^4 + b_4 \sum x_1^2 x_2^2 + b_5 \sum x_1^3 x_2$$

$$\sum x_2^2 y = b_o \sum x_2^2 + b_1 \sum x_1 x_2^2 + b_2 \sum x_2^3 + b_3 \sum x_1^2 x_2^2 + b_4 \sum x_2^4 + b_5 \sum x_1 x_2^3$$

$$\sum x_1 x_2 y = b_o \sum x_1 x_2 + b_1 \sum x_1^2 x_2 + b_2 \sum x_1 x_2^2 + b_3 \sum x_1^3 x_2 + b_4 \sum x_1 x_2^3 + b_5 \sum x_1^2 x_2^2$$

(a) Al 2024

Using simple program in Microsoft Excel, 6 simultaneous equations were obtained (all the coefficients were reduced by dividing with a_o's coefficient):

$$0.636 = b_0 + 0.692b_1 + 55b_2 + 0.538b_3 + 3675b_4 + 38.05b_5$$

$$0.561 = b_0 + 0.778b_1 + 55b_2 + 0.661b_3 + 3675b_4 + 42.78b_5$$

$$0.655 = b_0 + 0.692b_1 + 66.82b_2 + 0.538b_3 + 5134b_4 + 46.22b_5$$

$$0.501 = b_0 + 0.85b_1 + 55b_2 + 0.769b_3 + 3675b_4 + 46.73b_5$$

$$0.671 = b_0 + 0.692b_1 + 76.84b_2 + 0.538b_3 + 6396b_4 + 53.15b_5$$

$$0.581 = b_0 + 0.778b_1 + 66.82b_2 + 0.661b_3 + 5134b_4 + 51.98b_5$$

Solving the equations above simultaneously:

$b_0 = 1.42615$ $b_1 = -1.72283$ $b_2 = 1.47869 \times 10^{-3}$

$b_3 = 0.557488$ $b_4 = -4.39349 \times 10^{-6}$ $b_5 = 9.70874 \times 10^{-4}$

$\therefore$ The suitable regression function for Al 2024:

$$\frac{a}{S} = 1.42615 - 1.72283x_1 + 1.47869 \times 10^{-3} x_2 + 0.557488x_1^{\,2} - 4.39349 \times 10^{-6} x_2^{\,2} + 9.70874 \times 10^{-4} x_1 x$$

$$R^2 = 1 - \frac{\text{Unexplained variation}}{\text{Total variation}} = 1 - \frac{\sum (y - \hat{y})^2}{\sum (y - \bar{y})^2} = 1 - \frac{0.0366276}{0.616085} = 0.94$$

where

y = experimental value $\bar{y}$ = average of experimental values

$\hat{y}$ = predicted value from the regression equation

(b) Al 7150

Using simple program in Microsoft Excel, 6 simultaneous equations were obtained (all the coefficients were reduced by dividing with a_o's coefficient):

$$0.589 = b_0 + 0.692b_1 + 55b_2 + 0.538b_3 + 3675b_4 + 38.05b_5$$

$$0.510 = b_0 + 0.778b_1 + 55b_2 + 0.661b_3 + 3675b_4 + 42.78b_5$$

$$0.614 = b_0 + 0.692b_1 + 66.82b_2 + 0.538b_3 + 5134b_4 + 46.22b_5$$

$$0.446 = b_0 + 0.85b_1 + 55b_2 + 0.769b_3 + 3675b_4 + 46.73b_5$$

$$0.634 = b_0 + 0.692b_1 + 76.84b_2 + 0.538b_3 + 6396b_4 + 53.15b_5$$

$$0.534 = b_0 + 0.778b_1 + 66.82b_2 + 0.661b_3 + 5134b_4 + 51.98b_5$$

Solving the equations above simultaneously:

$b_0 = 1.11595$ $b_1 = -1.47162$ $b_2 = 8.61337 \times 10^{-3}$

$b_3 = 0.423993$ $b_4 = -4.7209 \times 10^{-5}$ $b_5 = -9.70874 \times 10^{-4}$

$\therefore$ The suitable regression function for Al 7150:

$$\frac{a}{S} = 1.11595 - 1.47162x_1 + 8.61337 \times 10^{-3} x_2 + 0.423993x_1^{\,2} - 4.7209 \times 10^{-5} x_2^{\,2} - 9.70874 \times 10^{-4} x_1 x_2$$

$$R^2 = 1 - \frac{\sum (y - \hat{y})^2}{\sum (y - \bar{y})^2} = 1 - \frac{0.03876569}{0.692283} = 0.94$$